Solid-State NMR Studies of Molecular Sieve Catalysts

JACEK KLINOWSKI

Department of Chemistry, University of Cambridge, Lensfield Road, Cambridge CB2 1EW, U.K.

Received April 1, 1991 (Revised Manuscript Received August 26, 1991)

Contents

1. Introduction 1459
2. Spectroscopic Considerations 1460
3. Composition of the Aluminosilicate Framework and the Nature of Extraframework Aluminum 1460
4. Resolving Crystallographically Nonequivalent Tetrahedral Sites 1462
5. Spectral Resolution, Line Shape, and Relaxation 1462
6. Dealumination and Realumination of Zeolites 1463
7. NMR Studies of the Structure of Brønsted Acid Sites 1466
8. Chemical Status of Guest Organics in the Intracrystalline Space 1469
9. In Situ Studies of Catalytic Reactions on Molecular Sieves 1471
10. Direct Observation of Shape Selectivity 1474

Jacek Klinowski was born in Kraków, Poland, on October 11, 1943. He has doctorates from the Jagiellonian University and from the University of London and is a Master of Arts of the University of Cambridge. Between 1969 and 1979 he worked with R. M. Barrer, FRS, a leading zeolite scientist, at Imperial College, London, and is now a member of the academic staff at the Chemistry Department in Cambridge. His interests include the structure and properties of molecular sieves, solid-state NMR spectroscopy, catalysis, and minimal surfaces. He has about 180 publications on these subjects, and is Editor-in-Chief of *Solid State NMR*, an international learned journal.

1. Introduction

Molecular sieves are a class of porous open-framework solids, which includes aluminosilicates (zeolites), aluminophosphates, and silicoaluminophosphates of diverse structures. Zeolites, the original molecular sieves, are built from corner-sharing SiO_4^{4-} and AlO_4^{5-} tetrahedra and contain regular systems of intracrystalline cavities and channels of molecular dimensions. The net negative change of the framework, equal to the number of the constituent aluminum atoms, is balanced by exchangeable cations, M^{n+}, typically sodium, located in the channels which normally also contain water. The name "zeolite" (from the Greek $\zeta\epsilon\omega$ = to boil and $\lambda\iota\theta o\sigma$ = stone) was coined by Cronstedt[1] in 1756 to describe the behavior of the newly discovered mineral stilbite which, when heated, rapidly loses water and thus seems to boil.

The general oxide formula of a zeolite is $M_{x/n}(AlO_2)_x(SiO_2)_y \cdot mH_2O$ where $y \geq x$. Aluminate tetrahedra cannot be neighbors in the frameworks of hydrothermally prepared zeolites, i.e. Al–O–Al linkages are forbidden. This requirement is known as the Loewenstein rule.[2] There are at present around 40 identified species of zeolite minerals (with $1 \leq y/x \leq 5$) and at least 125 synthetic species with a very wide range of aluminum contents.

Zeolites are prepared under mild (60–400 °C) hydrothermal conditions in strongly basic media. The type and concentration of the base are important structure-directing factors and a variety of organic bases are now being used in zeolite synthesis. The ZSM series (for Zeolite Socony Mobil) of highly siliceous zeolites is prepared from solutions containing alkylammonium bases. Other elements, such as Ga, Ge, B, Fe, and P can substitute for Si and Al in the framework, and there are claims that many other elements can also do so.

Zeolites have a number of interesting physical and chemical properties. The three classes of phenomena which are of greatest practical importance are the ability to sorb organic and inorganic substances, to act as cation exchangers and to catalyse a wide variety of reactions.

The zeolitic channel systems, which may be one-, two- or three-dimensional and may occupy more than 50% of crystal volume, are normally filled with water. When water is removed, other species such as gaseous elements, ammonia, alkali metal vapors, hydrocarbons, alkanols, and many other organic and inorganic species may be accommodated in the intracrystalline space. Depending on pore diameter and on molecular dimensions, this process is often highly selective, and gives rise to the alternative name for zeolites: molecular sieves. Thus zeolitic sorption is a powerful method for the resolution of mixtures. Commercial applications include thorough drying of organics, separation of hydrocarbons and of N_2 and O_2 in air and the removal of NH_3 and CS_2 from industrial gases.

Cations neutralizing the electrical charge of the aluminosilicate framework can be exchanged for other cations from solutions. Zeolites often possess high ion-exchange selectivities for certain cations, and this is used for their isolation and concentration. Molecule sieving properties of zeolites can be further modified by ion exchange. Thus Na–A sorbs both N_2 and O_2

0009-2665/91/0791-1459$09.50/0 © 1991 American Chemical Society

while Ca-A sorbs nitrogen preferentially to oxygen.

However, it is the ability to catalyze a wide range of reactions, such as cracking, hydrocracking, oxidation, and isomerization of hydrocarbons, which by far overshadows all other applications of zeolites. Rare-earth exchanged and hydrogen forms (prepared indirectly by thermal decomposition of the ammonium form) of some zeolites, such as zeolite Y, mordenite, gmelinite, and chabazite, have a cracking activity which is orders of magnitude greater than that of conventional silica/alumina catalysts. Zeolite-based catalysis was first discovered[3] in 1960 and two years later cracking catalysts based on zeolite Y were introduced. They have now almost completely displaced conventional catalysts. The synthetic zeolite ZSM-5, introduced in 1972,[4] is an even more powerful catalyst. Its high silica content (Si/Al ratio is typically 30) gives it high thermal stability, while the channel diameter is very convenient for many applications, particularly in the petroleum industry. The 10-membered channels of ZSM-5 are responsible for the quite striking shape selectivity. Catalytic properties of ZSM-5 include the ability to synthesize gasoline from methanol in a single step. Silicalite, a material which is isostructural with ZSM-5, but contains only small amounts of aluminum is, by contrast to most other zeolites, nonpolar (i.e. hydrophobic) and organophilic. Silicalite is used in the removal of dissolved organics from water.

Since 1982 several new families of porous solids have been synthesized. The $AlPO_4$ molecular sieves, with structures built from alternating AlO_4^{4-} and PO_4^{4-} tetrahedra, were the first to be discovered.[5] Some of them have the framework topologies of known zeolites, but many have novel structures. $AlPO_4$ materials are synthesized from gels containing sources of aluminum, phosphorus, and at least one organic structure-directing template. Incorporation of a silicon source into an aluminophosphate gel results in the formation of silicoaluminophosphates, SAPO, and the incorporation of a metal, Me (such as Mg, Mn, Fe, Co, or Zn), into $AlPO_4$ and SAPO gives the MeAPO and MeAPSO sieves, respectively.[6] Some of these have high Brønsted acidities and thus a considerable potential as heterogeneous catalysts. Specialist monographs and numerous reviews on the structure and properties of molecular sieves are available.[7-19]

Synthetic zeolites are usually microcrystalline and furthermore typically contain *four* 10-electron atomic species (Si^{4+}, Al^{3+}, O^{2-}, and Na^+) which makes them difficult to study by conventional techniques of structural elucidation. The development of high-resolution solid-state NMR techniques, such as magic-angle spinning (MAS), gave zeolite chemistry a powerful structural tool to monitor all elemental components of such frameworks.

The aim of this review is to survey solid-state NMR results, particularly recent, which are of direct relevance to heterogeneous catalysis on molecular sieves. I shall consider in turn the following factors which influence catalytic activity:

(a) The composition and ordering of the framework, and its modification by dealumination and realumination

(b) Nature and quantity of extraframework Al

(c) Chemistry of the Brønsted acid sites

(d) Chemical status of guest organics in the intracrystalline space

(e) Shape selectivity

2. Spectroscopic Considerations

^{29}Si, ^{27}Al, ^{31}P, and ^{17}O have been observed in the frameworks of molecular sieves by using MAS NMR. In particular, ^{29}Si studies have provided many new insights into the structure and chemistry of zeolites. Signals originating from crystallographically inequivalent silicon atoms can now be resolved and related to structural parameters.

The full range of ^{29}Si chemical shifts is over 500 ppm wide, but most shifts are found in a narrower range of ca. 120 ppm. Pioneering studies in *high-resolution* solid-state ^{29}Si NMR spectroscopy have been performed by Lippmaa et al., who carried out the first comprehensive investigation[20] of a variety of silicates and aluminosilicates.

In principle, ^{27}Al is a very favorable nucleus for NMR: it has a 100% natural abundance with a chemical shift range of about 450 ppm. However, it is a quadrupolar nucleus (spin $^5/_2$) and the quadrupole interaction is usually large, which broadens and shifts the resonance lines. With quadrupolar nuclei of noninteger spin, the central transition, the only one which is normally observed, is independent of the quadrupolar interaction to first order, but is affected by second-order effects which are inversely proportional to the magnetic field strength. The best spectra are obtained at very high magnetic fields and with fast magic-angle spinning. It has been shown[21-26] that it is essential to use strong radio frequency pulses with small flip angles to obtain quantitatively reliable spectra. Similar considerations apply to ^{23}Na, a 100% abundant spin $^3/_2$ nucleus.

Because of the large quadrupolar interactions affecting ^{27}Al, the detection and quantification of aluminum in solids by NMR is often difficult. This has seriously hindered NMR studies of the $AlPO_4$ molecular sieves, which often show very large quadrupolar effects as well as strong interactions with water and other adsorbates. The development of double rotation (DOR) is a major advance in the study of quadrupolar nuclei, as it removes not only first-order broadening effects such as chemical shift anisotropy, but also second-order quadrupolar interactions.[27,28] DOR has been applied to study of the very large pore aluminophosphate VPI-5, as well as $AlPO_4$-11 and $AlPO_4$-21/25.[29]

High-resolution ^1H MAS NMR is a powerful tool for the measurement of zeolitic acidity. In general, the difficulties involved in high-resolution proton work in the solid state are (a) the strong dipolar interactions and (b) the narrow range of ^1H chemical shifts. The consequence of this is that only a limited number of NMR signals can be resolved. Fortunately, the protons in dehydrated zeolites are usually relatively far apart, which considerably reduces the dipolar interaction. As a result, important NMR information on the chemical status of hydroxyl groups in zeolites has been obtained.

3. Composition of the Aluminosilicate Framework and the Nature of Extraframework Aluminum

Framework Si in zeolites is tetrahedrally coordinated, and thus there are five different possible environments

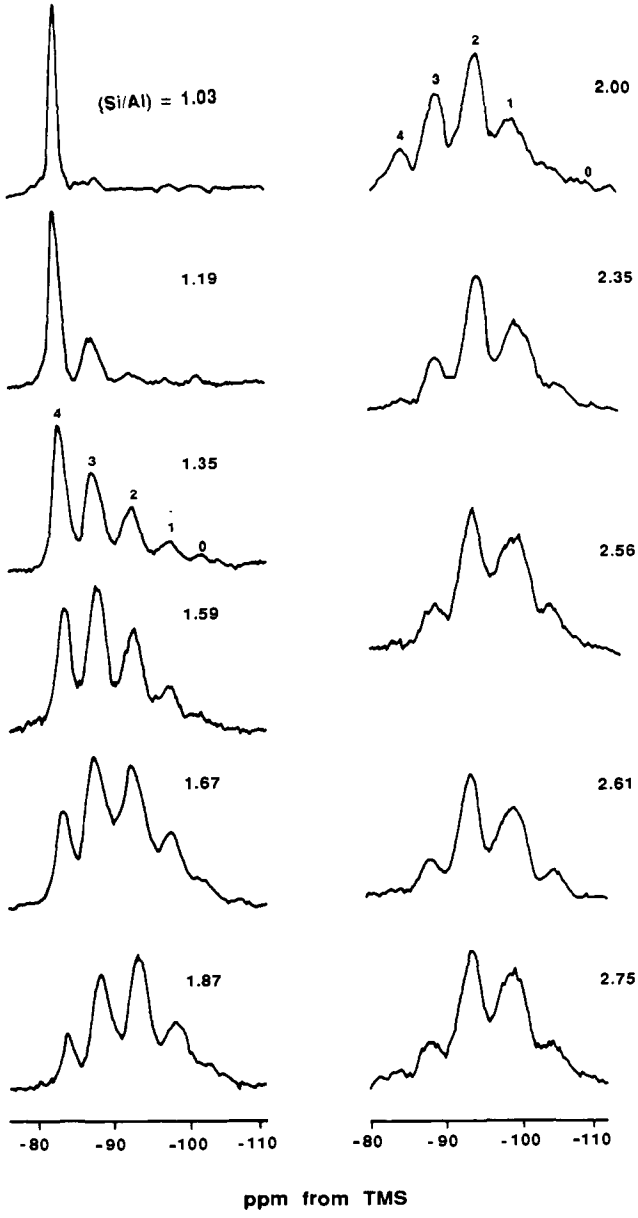

Figure 1. High-resolution ^{29}Si MAS NMR spectra of synthetic zeolites NaX and NaY.[34] Si(nAl) signals are identified by the n above the peaks.

of a silicon atom denoted as Si(nAl) where n ($\leq$4) signifies the number of aluminum atoms connected, via oxygens, to a silicon. Each type of Si(nAl) building block corresponds to a definite range of ^{29}Si chemical shift. When a ^{29}Si MAS NMR spectrum of a zeolite (a) contains more than one signal and (b) is correctly assigned in terms of Si(nAl) units, the Si/Al ratio *in the zeolitic framework* may be calculated from the spectrum alone. This method is valid because in the absence of Al–O–Al linkages the environment of every Al atom is Al(4Si). Therefore, each Si–O–Al linkage in an Si(nAl) unit incorporates 0.25 Al atoms, and the whole unit 0.25n Al atoms. The Si/Al ratio in the aluminosilicate framework may be calculated directly from the ^{29}Si MAS NMR spectrum using the formula[30,31]

$$(\mathrm{Si/Al})_{\mathrm{NMR}} = \frac{I_4 + I_3 + I_2 + I_1 + I_0}{I_4 + 0.75I_3 + 0.5I_2 + 0.25I_1} \quad (1)$$

where I_n denotes the intensity (peak area) of the NMR signal corresponding to the Si(nAl) building unit. By

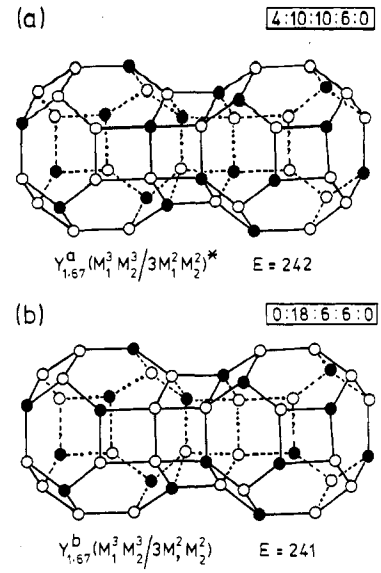

Figure 2. Two of the possible Si,Al ordering schemes for zeolite Y with Si/Al = 1.67.[34] Open circles denote Si atoms, closed circles Al atoms. The ratio of intensities S(4Al):Si(3Al):Si(2Al):Si(1Al):Si(0Al) corresponding to each scheme is given in the upper right-hand corner. E is the calculated electrostatic energy for the double cage in units of $(qe)^2/a$, where a is the T–O–T distance. The asterisk denotes the preferred scheme.

comparing $(\mathrm{Si/Al})_{\mathrm{NMR}}$ values with the results of chemical analysis, which gives *bulk* composition, the amount of extraframework aluminum can be calculated, which is important when dealing with chemically modified zeolites.

Equation 1 is independent of structure and applies to all zeolites provided the assumptions made in its derivation are justified. It can, by implication, serve as a test for the correctness of spectral assignment. Its validity has been tested in the case of zeolites X and Y and their gallosilicate equivalents, which can be synthesized in a range of compositions. The spectra can be deconvoluted by computer using Gaussian peak shapes, and the areas of the individual deconvoluted signals used in (1). Very good agreement was found between the Si/Al ratios obtained by chemical analysis and those calculated from the spectra. Equation 1 works well with materials which have framework Si/Al ratios less than about 10. However, it cannot be directly applied to spectra containing overlapping signals from Si(nAl) units of crystallographically nonequivalent Si atoms.[31-33]

^{29}Si NMR is of considerable assistance in determining the *ordering* of Si and Al atoms in the framework, beyond the restrictions of the Loewenstein rule. The areas under the peaks in the (deconvoluted) spectrum are directly proportional to the populations of the respective structural units in the sample. It is therefore possible to estimate these from the experimental data (see Figure 1) and to compare them with the relative numbers of such units contained in models involving different Si,Al ordering schemes. Klinowski et al.[34] found that for most Si/Al ratios more than one ordering scheme is compatible with the Si(nAl) intensities determined by ^{29}Si MAS NMR. They chose between the various schemes on the basis of (a) the degree of agreement between the *actual* spectral intensities and those required by the given model, (b) compliance with crystal symmetry requirements, and (c) minimum

electrostatic repulsion within the aluminosilicate framework. Figure 2 shows the preferred ordering schemes for Si/Al = 1.67. Engelhardt et al.[30] and Melchior et al.[35] came to very similar conclusions.

4. Resolving Crystallographically Nonequivalent Tetrahedral Sites

In naturally occurring zeolites the Si/Al ratio is always less than about 5, but materials with much lower Al contents can be prepared in the laboratory. One of them, known as ZSM-5, has Si/Al ratio between 20 and many thousand and possesses remarkable catalytic properties (see below). A crystalline microporous material called silicalite, isostructural with ZSM-5 but containing only traces of Al, has also been prepared.

In the light of the previous discussion about the appearance and interpretation of ^{29}Si MAS NMR spectra of zeolites, one might expect an uncomplicated spectrum for a highly siliceous zeolite, displaying the Si(4Al) signal, sometimes with a smaller Si(3Al) resonance depending on the Si/Al ratio. The spectrum of a typical sample of as-prepared ZSM-5 is indeed almost featureless. The discovery[36] that the spectrum of a sample of silicalite with a particularly low Al content shows considerable fine structure was therefore a surprise. The chemical shifts of *all* the peaks are characteristic of Si(4Si) groupings in highly siliceous materials. The observed multiplicity arises from crystallographically inequivalent tetrahedral environments of the Si(4Si) sites. Fyfe et al.[37] subsequently obtained a spectrum of silicalite of even higher resolution in which as many as 20 individual lines can be separately resolved and the line width of the narrowest line is ca 5 Hz, which brings it close to the realm of high-resolution NMR in liquids. The spectrum may be simulated by 20 Gaussian signals, and the total intensity of the spectrum is 24 times greater than the intensity of the smallest signal. This indicates that the space group of silicalite contains 24 nonequivalent sites in the unit cell. X-ray diffraction (XRD) studies indicate that silicalite can exist in the monoclinic and the orthorhombic forms and that the slight changes of symmetry involved are related to the residual aluminum content. The same structural transformation was also found to be reversibly temperature induced, the "low" temperature form being monoclinic and the "high" temperature form, orthorhombic. ^{29}Si MAS detects much more subtle changes in the structure of silicalite: minute variations in atomic positions[37-40] which do not necessarily involve symmetry changes detectable by XRD. Spectra measured in the range 153–403 K are sensitive even to small temperature changes and reveal that structural transformations continue over the entire range. By contrast, the changes in the XRD pattern are slight. This demonstrates the remarkable sensitivity with which NMR can monitor relatively minor modifications in atomic positions. It is interesting to note that the addition of very small amounts of adsorbed organic molecules to dehydrated silicalite induces similar phase transitions and similar, but not identical, changes in the ^{29}Si spectra.[41-43]

Two-dimensional solid-state NMR techniques have been used to assign the individual NMR signals to specific crystallographic sites. In particular, two-dimensional homonuclear correlation spectroscopy (COSY), well established for the study of liquids, has recently been shown to be feasible with zeolitic samples.[44-49] The experiment relies on coherence transfer, which in the solid state may occur through dipolar or scalar couplings. The latter possibility has been exploited more often, as in favorable circumstances it allows the chemist to establish atomic connectivities unambiguously. However, several factors impose severe restraints on the COSY experiment in the solid state.

First, since one observes a dilute nucleus embedded in a crystal lattice, cross-peaks due to coupled spins are much less intense than diagonal peaks which originate mostly from isolated spins. The result is that intense diagonal peaks can swamp the weaker cross-peaks. Isotopic enrichment in ^{29}Si was found to be a useful remedy.[44,45] Second, most 2D NMR methods in solids suffer from low sensitivity because of fast transverse relaxation. In particular, in the COSY experiment the spin system must evolve for a sufficiently long time in both dimensions in order to obtain adequate cross-peaks intensities. To overcome this difficulty, Fyfe et al.[44,45] introduced two extras delays into their solid-state COSY pulse sequence, an idea which had originally been used in the so-called "long range" or "delayed" COSY in liquids.[50]

Finally, attempts have been made to overcome the problem of intense diagonal signals stemming mostly from isolated spins. These can be removed in the INADEQUATE experiment,[51,52] which is, however, very insensitive even in liquids and requires an accurate estimation of the coupling constants.[53] Besides, in the solid state the disadvantage of the rapid transverse relaxation is more acute in INADEQUATE which uses a longer pulse sequence than conventional COSY. Despite this, there have been several successful ^{29}Si 2D INADEQUATE experiments in the solid state on highly siliceous zeolites including ZSM-5.[46-49,54] Excitation of a double quantum coherence can also be used in double-quantum filtered COSY. The only experiment of this type used a ^{29}Si-enriched sample of the highly siliceous zeolite ZSM-39.[45]

5. Spectral Resolution, Line Shape, and Relaxation

The earliest ^{29}Si MAS NMR spectra of zeolites, measured in a magnetic field of 2.35 T or lower, showed modest resolution. The considerable improvement in resolution upon increasing the field must therefore be due to the removal of some field-dependent effect. Resolution increases until a field of about 4.70 T is reached, and no further improvement is observed (as opposed to a continuing increase in the signal-to-noise ratio) above this value. Dipolar ^{29}Si–^{29}Si coupling is unlikely to be responsible, in view of (a) the magnetic dilution of the ^{29}Si nucleus, (b) the weakness of such coupling, which is in any case removable by MAS, and (c) the fact that dipolar interactions are field independent. Melchior[55] suggested that the likely cause is the ^{29}Si–^{27}Al dipole–quadrupole interaction. Such interaction gives rise to splitting and broadening of ^{13}C MAS NMR spectra of α-carbon atoms in amino acids, effects which disappear when ^{14}N (spin 1) is substituted by ^{15}N (spin $^1/_2$). In zeolites an analogous effect is caused by the deviation of the quantization axis for ^{27}Al from the direction of the applied magnetic field caused by the quadrupolar interaction. The dipolar Hamilto-

nian then contains angle-dependent terms other than $(3\cos^2\theta - 1)$ and is not averaged to zero by MAS. It has been shown that these interactions, which are inversely proportional to the cube of the internuclear distance, are also strongly dependent on the magnetic field. It seems likely that the ^{29}Si–^{27}Al coupling is significant mainly in Si(nAl) units with $n > 0$ [note that the Si(4Si) signal is narrow even at low fields] and that it is eliminated in the fields of 4.7 T or larger.

It has been shown above that the removal of Al from the zeolitic framework leads to very marked narrowing of NMR signals. When no Al is present, the Si(4Si) lines from silicalite/ZSM-5 are very narrow indeed. Fyfe et al.[37,43] studied the effect of dealumination on line widths of Si(4Si) signals in several zeolites. They found that substantial line narrowing occurs at Si/Al > 100, concluded that the effect must be long range in nature, and suggested that it is caused by a chemical shift interaction due to distribution of Al in the second nearest and further coordination shells of silicon.

Hamdan and Klinowski[56] questioned this hypothesis. They agree that dealumination does simplify ^{29}Si spectra of zeolites by (a) eliminating Si(nAl) sites with $n > 0$ and (b) reducing the number of Al atoms in the second and further tetrahedral coordination shells of silicon. But they also point out that the extraordinary thoroughness of heat treatment required for good spectral resolution in ZSM-5/silicalite does not support the chemical shift mechanism of line narrowing: the resolution of a sample with Si/Al = 125 (corresponding to the average Si–Al distance of 8.9 Å) is poor, while the sample with Si/Al = 300 gives a well-resolved spectrum, although the Si–Al distance is 11.9 Å, i.e. not drastically greater. Furthermore, silicalite obtained via the so-called "fluoride" method and containing the same level of Al impurities, as well as an *aluminated* sample (see below) with Si–Al distance of only 5.0 Å give highly resolved spectra. It is likely that improved spectral resolution is due to a process, such as healing of structural defects, which occurs *in parallel* with dealumination during hydrothermal treatment.

^{29}Si spin–lattice relaxation times, T_1, in zeolites are relatively short in comparison with those for ^{13}C in organic solids. T_1 values of 5–30 s have been measured in various zeolites. It was also found that, for a given zeolite, T_1 of a silicon atom in a Si(nAl) unit varies little with n, and is also insensitive to a change in the Si/Al ratio. This indicates that relaxation is not affected by the presence of ^{27}Al and also explains why short recycle times used by most workers (typically 5 s, i.e. much shorter than $5T_1$) still give quantitatively reliable spectra.

It was often assumed that spin–lattice relaxation in zeolites is controlled by spin diffusion from paramagnetic centers. However, this mechanism is likely to be very inefficient in view of the large distance between neighboring silicons, the relatively low abundance of ^{29}Si, and the "detuning" influence of ^{27}Al. Also, the "impurity" hypothesis cannot explain why T_1 for synthetic zeolites with very low levels of paramagnetics remains short nor, why upon rendering a zeolite amorphous, T_1 increases by orders of magnitude while the concentration of paramagnetic component remains constant. Klinowski et al.[57] measured the T_1 of a number of zeolites contained in sealed capsules under oxygen and argon atmospheres and found that the effect of oxygen is dramatic, while water and paramagnetic impurities play a secondary role in relaxation. For dealuminated mordenite T_1 is reduced by 3 orders of magnitude in comparison with the value under argon. Furthermore, relaxation times of crystallographically nonequivalent Si atoms often differ significantly within the same sample. These results offer an explanation why T_1 increases so dramatically when the zeolite is made amorphous and why relaxation in compact silicates (such as quartz) and glasses is so slow. It is simply that most Si atoms in such samples are inaccessible to oxygen. It also seems likely that the significant lengthening of T_1 upon addition to zeolites of various organic materials is due to the displacement of oxygen from the intracrystalline space by the guest molecules and that reports of a major influence of dehydration of the zeolite on the T_1 of ^{29}Si stem from the failure to separate the effects of *dehydration* and *evacuation*. The results of ref 57 (a) offer a means of rapid acquisition of ^{29}Si NMR spectra of zeolites, (b) suggest a new, quantitatively reliable method for the study of surfaces of amorphous silicas, silica-aluminas and silicate glasses, and (c) provide a method of obtaining site-selective spectra via careful control of the partial pressure of oxygen.

Haase et al.[58] found that spin–lattice relaxation times of ^{27}Al in zeolitic frameworks are between 0.3 and 70 ms depending on temperature. The relaxation is governed by the electric quadrupole interaction with the crystal electric field gradients modulated by translational motion of *polar sorbate molecules* and charge-compensating cations. For example, relaxation times in zeolite NaX were unchanged upon replacing $^2/_3$ of intracrystalline H_2O by D_2O while the overall pore-filling factor was unchanged. Since ^1H and ^2H have very different gyromagnetic constants, spin–lattice relaxation of ^{27}Al cannot be caused by the magnetic dipole interaction with ^1H of the water molecules. Furthermore, T_1 dramatically increases upon dehydration of the sample, which demonstrates that the controlling mechanism in hydrated samples must be the *quadrupolar* interaction of ^{27}Al with the crystal electric field gradient produced by the very similar electric dipole moments of the H_2O and D_2O molecules. Dipolar interactions with paramagnetic impurities become significant as a ^{27}Al relaxation mechanism only at very low temperatures.

6. Dealumination and Realumination of Zeolites

Since Brønsted acid groups in zeolites are associated with 4-coordinated framework aluminum, their catalytic activity strongly depends on the concentration and location of Al in the structure. The aluminum content of the zeolitic framework can be decreased by a number of methods. Upon hydrothermal treatment of zeolite NH_4-Y, the process known as "ultrastabilization",[59] part of the aluminum is ejected from the framework into the intracrystalline space, and the framework vacancies are reoccupied by silicon from other parts of the crystal. As a result, thermal stability of the zeolite is greatly increased, so that the product retains crystallinity at temperatures in excess of 1000 °C. Ultrastable zeolite Y has been extensively examined by ^{29}Si and ^{27}Al solid-state NMR.[60-69] Samples subjected to different types

of treatment have been examined, while the Si/Al ratio were determined from spectral intensities using (1). ^{29}Si NMR clearly shows[60,61] that Al is removed from the framework and that the resulting vacancies are subsequently reoccupied (see below). Chemical analysis shows no change in composition: the "missing" Al is now in 6-coordination, and there is a consequent loss of ion-exchange capacity. Other zeolites also undergo ultrastabilization during which Al is isomorphously replaced by Si.

While refs 60 and 61 establish the reoccupation of the framework vacancies, the questions of the precise mechanism of Al removal, the nature of the intermediate defect structure and of the origin of the Si for lattice reconstitution remain. Gas sorption studies[70] indicate that ultrastable zeolite Y contains a secondary mesopore system with pore radii in the range 15–19 Å, suggesting that tetrahedral sites are reconstituted with silicon which, contrary to earlier speculations, does not come only from the surface or from amorphous parts of sample, but also from its bulk, which may involve the elimination of the entire sodalite cages.

Engelhardt et al.[62] used ^{27}Si MAS NMR with cross-polarization (CP) in order to detect "surface" Si atoms attached to one or two hydroxyl groups. From spectra without CP they determined, using (1), framework Si/Al ratios, and by difference with the results of chemical analysis, the amount of nonframework Al. Si(3Si)(OH) groups were found at −100 ppm, and Si(2Si)$(OH)_2$ at −90.5 ppm, although the former signal coincides with that of Si(1Al,3Si) groupings. Zeolite Y treated hydrothermally at 540 °C for 3 h shows the presence of Si(3Si)(OH) groups due to defect sites in the CP spectrum, although their absolute amounts could not be determined because the enhancement factor (CP efficiency) is not known. When the so treated sample is extracted with 0.1 M HCl at 100 °C, not only interstitial but also framework Al is removed and many "hydroxyl nests" are formed. They cannot be healed, as at such a low temperature migration of silicon-bearing species must be insignificant. For repeatedly deep-bed-treated and acid-extracted samples, ^{29}Si spectra with and without CP are similar, which indicates that almost all vacancies are healed.

The extent of dealumination was found[63] to be limited by the degree of ammonium exchange of the starting material, and also to depend on the temperature and water vapor pressure during treatment. Depending on the conditions, any desired composition of the product can be obtained and no preferred Si/Al ratios were found. For a given temperature, the degree of dealumination increases approximately linearly with the degree of NH_4 exchange, but with a different slope for each temperature. The degree of dealumination is always far below the degree of exchange which indicates that a considerable number of acidic protons ("structural OH groups" produced by the decomposition of NH_4^+) must be retained. At low water vapor pressures, the extent of dealumination is limited by the availability of water.

Engelhardt et al.[64] considered the problem of Si,Al ordering in dealuminated zeolites Y in the range of compositions ($2.5 \leq Si/Al \leq 5.8$). They found that the relative spectral intensities are independent of the method of dealumination (shallow- or deep-bed, acid extraction) or conditions of thermal treatment, but depend only on the final value of Si/Al ratio. This does not necessarily mean that the ordering is the same, although this is a strong possibility. This is because "random" distribution and various different ordering schemes may in principle give rise to the same relative spectral intensities.

Bosáček et al.[65] used wide-line ^{27}Al NMR measurements of stationary samples to measure the parameters of the electric field gradient (EFG) at the nuclear site in decationated zeolites. In zeolite Na-Y they measured a line half-width of $\delta\nu_{1/2}$ = 61 kHz (for ν_L = 16 MHz) which leads, via the theoretical considerations to ν_Q = 840 kHz; the calculated field gradient was 2.9 V/Å^2. In hydrated samples this gradient is partially averaged by random reorientation of water molecules, giving $\delta\nu_{1/2}$ = 5.7 kHz and ν_Q = 256 kHz.

Freude et al.[66] carried out a systematic study of the relative amounts of 4- and 6-coordinated Al in thermally treated zeolite Y, using wide-line and MAS ^{27}Al NMR at 16 and 70.34 MHz, respectively. They found that loss of ^{27}Al line intensity takes place in treated zeolites in comparison with the parent material, evidently due to extraframework Al being in an environment of low symmetry.

It is of interest to consider the possible status of this "invisible" aluminum. It could be present as $Al(OH)_3$, $Al(OH)_2^+$, $Al(OH)^{2+}$, Al_2O_3, or some polymeric aluminous species. Freude et al.[66] suggested that the hydroxide is unlikely to be present in stabilized zeolites, which are strong solid acids, as it is not favored in acidic aqueous solutions. The "low symmetry environment" may be the surface of the crystallites or of the secondary pore system. Indeed, Lohse and Mildebrath[71] found Al_2O_3 clusters inside the mesopore system formed as a result of the proposed "condensation of lattice defects" during thermal treatment, while Dwyer et al.[72,73] and Ward and Lunsford[74] reported an enrichment in Al at the external surface of the particles of ultrastable zeolite Y using techniques other than NMR. Later work has shown that special care needs to be taken to obtain quantitatively reliable spectra of nonframework aluminum.[21–26] ^{27}Al MAS NMR shows how 6-coordinated nonframework Al species (Al^{NF}) build up at the expense of the 4-coordinated framework Al (Al^F) as the calcination temperature is increased.

^{27}Al quadrupole nutation NMR[77–81] (see below) suggests that the Al^{NF} signal at ca. 30 ppm (see Figure 3) has a large quadrupolar coupling constant (>6 MHz) for dealuminated samples with $(Si/Al)_{NMR}$ ratios between 5.2 and 20. Samoson et al.[78] concluded that it is not an independent resonance but the low-frequency component of a second-order quadrupolar line shape, the high-frequency counterpart of which overlaps with the Al^F signal at ca. 60 ppm. However, others[82,83] assigned resonances in the range 27–30 ppm in aluminosilicates to 5-coordinated Al. In order to elucidate the nature of Al^{NF}, ^{1}H–^{27}Al CP/MAS NMR spectra of samples of the dealuminated samples were recorded.[75–77] Figure 3 clearly shows that the intensity of the signals at 0 and 30 ppm increases relative to the signal at 60 ppm. This indicates that the 30 ppm signal is a separate ^{27}Al resonance. Furthermore, the position of NMR signals in ^{27}Al MAS NMR spectra reported in ref 78, recorded at the higher field of 11.7 T (as opposed to 9.4

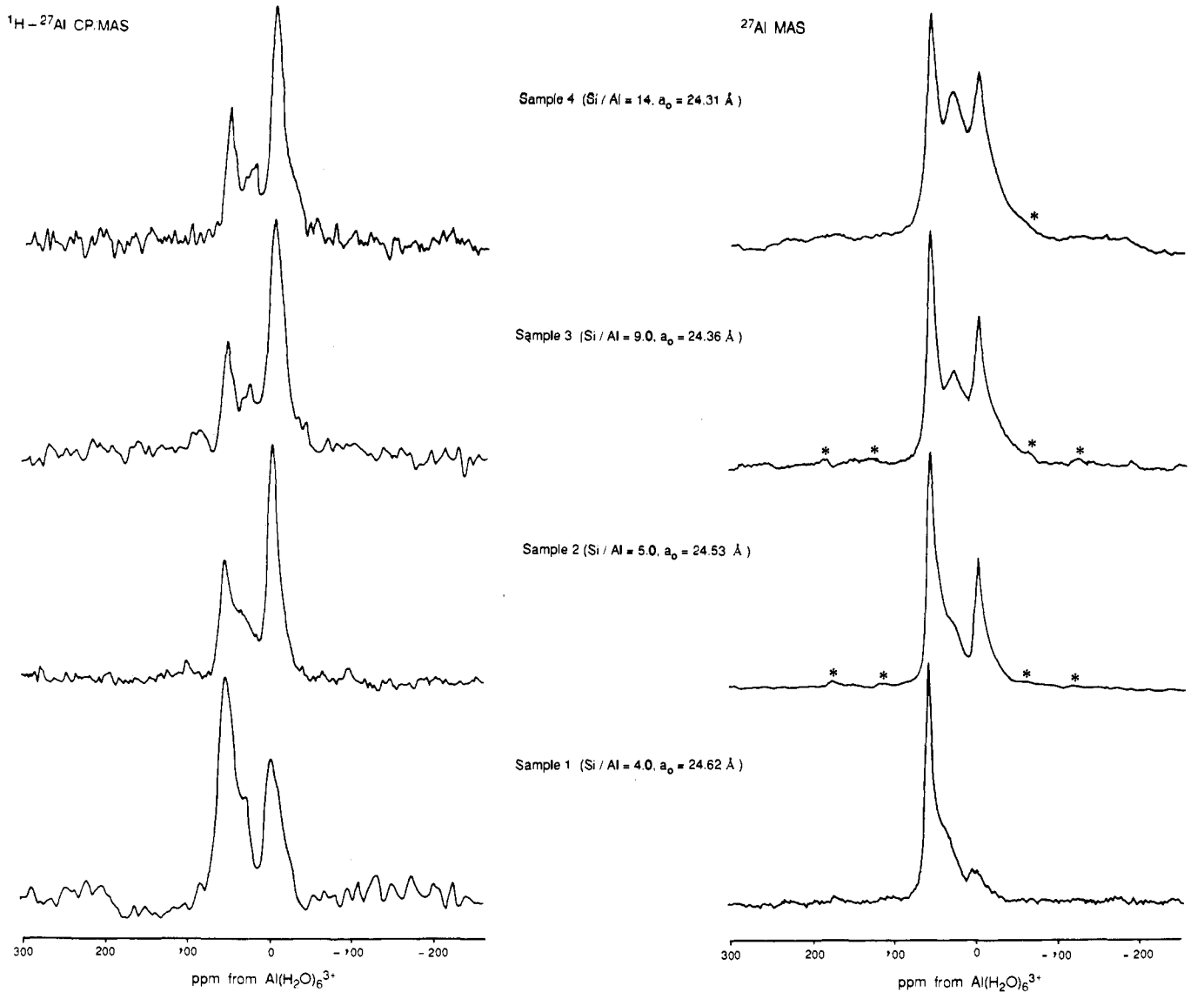

Figure 3. ^{27}Al (MAS at 12–13 kHz) and $^1H-^{27}Al$ CP/MAS (MAS at 8–10 kHz) NMR spectra of increasingly dealuminated (from bottom to top) zeolite HY.[76] The Si/Al ratios calculated from ^{29}Si MAS NMR spectra and the unit cell parameters, a_0, are indicated. Asterisks denote spinning sidebands.

T in refs 76 and 77), is the same at 0, 30, and 60 ppm. As the second-order quadrupole interaction is inversely proportional to the magnetic field, components of a quadrupolar line shape must shift to high frequency when the magnetic field is increased. Since the distance between peaks is unchanged, it was concluded that they correspond to independent resonances.

The ^{27}Al CP/MAS spectrum of zeolite Na-Y (not shown) contains two very faint signals at 61 and 9 ppm, presumably due to a small amount of impurity. These signals are 1 order of magnitude weaker than the signals in the spectrum of dealuminated Y shown in Figure 3. A signal at ca. 60 ppm is clearly seen in the $^1H-^{27}Al$ CP/MAS spectrum of dealuminated zeolite Y, probably associated with 4-coordinated nonframework Al. The possibility that two (or more) ^{27}Al resonances overlap at ca. 60 ppm must therefore be considered. In fact, quadrupole nutation studies have previously given some support for the presence of 4-coordinated Al^{NF} in dealuminated zeolite Y.

The process of ultrastabilization can be completely reversed by a simple hydrothermal treatment with aqueous solutions of strong bases.[84-85] The reaction can be profitably studied by NMR, which indicates that aluminum atoms hydrothermally eliminated from the framework of zeolite Y can be subsequently reinserted into the framework. Sample crystallinity is largely retained in the process, and is strongly dependent upon the residual sodium content of the parent material, the concentration of the base and the temperature.

^{29}Si MAS NMR spectra of dealuminated samples (middle traces in Figure 4) indicate the removal of framework aluminum from the parent sample (top trace). However, the spectra of samples treated with KOH (lower traces) are dramatically different. The intensities of the Si(0Al) signals are greatly reduced, and the intensities of the Si(1Al), Si(2Al), Si(3Al), and Si(4Al) signals correspondingly increased, signifying that a considerable amount of aluminum has entered the framework. Using values of $(Si/Al)_{NMR}$ calculated from (1) in conjunction with the values of the *overall* Si/Al ratio measured by X-ray fluorescence we can calculate the number of framework and nonframework atoms per unit cell. The results show that all extraframework Al atoms in samples 2, 4, and 6 have reentered the framework to give realuminated samples 3,

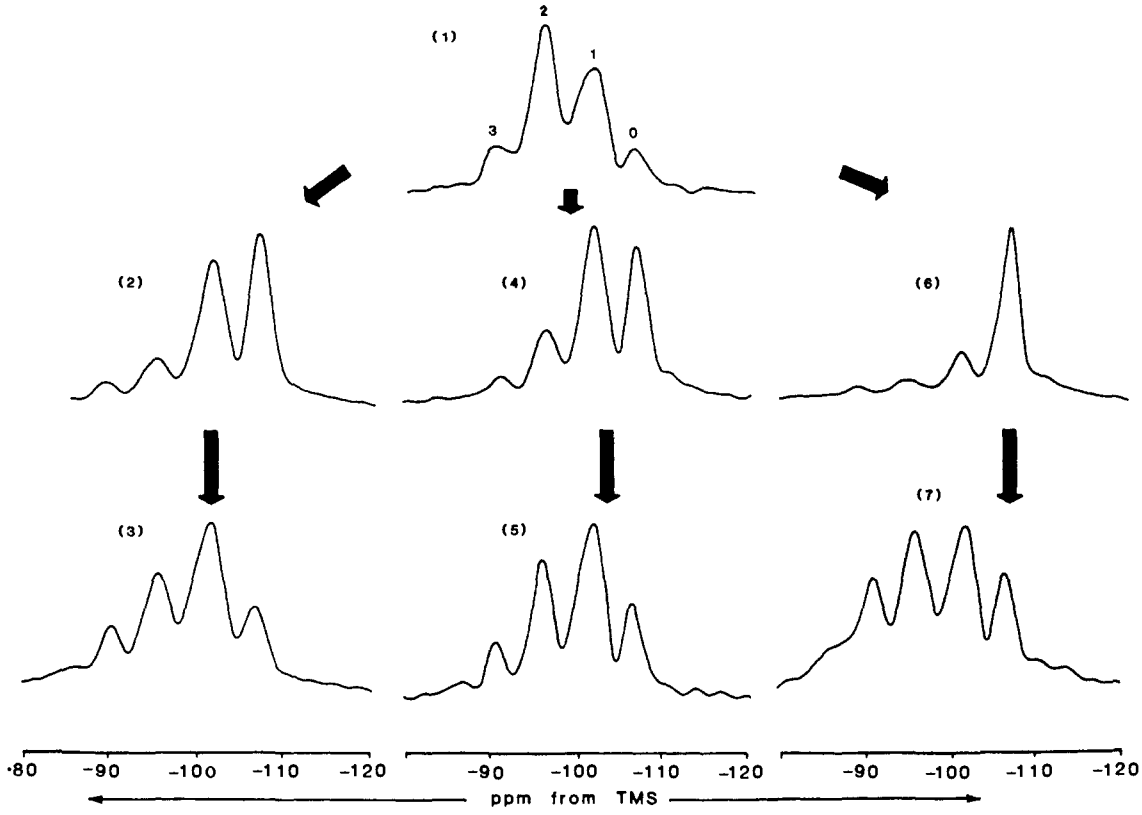

Figure 4. ^{29}Si MAS NMR spectra of ultrastabilized and hydrothermally realuminated zeolites for the single ultrastabilization/realumination cycle.[84] Sample 1 (Si/Al = 2.56) is the parent for samples 2, 4, and 6 (Si/Al ratios 4.96, 4.26, and 7.98 respectively), which upon treatment with KOH solution give rise to samples 3, 5, and 7 (Si/Al ratios of 2.44, 2.70, and 2.09), respectively. Numbers above individual peaks give the n in Si(nAl).

5, and 7, respectively. Furthermore, the spectra of the realuminated samples are very different from that of the parent sample 1 despite the fact that the composition of all four samples is similar. This shows that although the overall structure of the crystal is known exactly, the Si,Al *distribution* among the tetrahedral sites is different in each case.

^{27}Al quadrupole nutation NMR offers insights into the dealumination–realumination process. In this technique,[78-81] a series of free induction decays during the interval t_2 is acquired using powerful resonant radio frequency pulses while monotonically increasing the length, t_1, of the pulse. Double Fourier transformation in t_2 and t_1 gives a two-dimensional nutation NMR spectrum (in the magnitude mode) with the axes F_2 (containing combined chemical shift and the second-order quadrupole shift) and F_1 (containing quadrupolar information only). The technique permits ^{27}Al sites with different quadrupole coupling constants to be resolved along F_1.

The nutation spectrum of the parent sample 1 (Figure 5) consists of two signals, at 60 ppm, 78 kHz and 60 ppm, 195 kHz, both with the same line width and both corresponding to framework (F) aluminum. The presence of *two* signals is due to the fact that the quadrupole interaction characteristic of framework ^{27}Al is of the same order of magnitude as the strength of the rf pulse. Sample D-1 has been mildly, and sample D-2 strongly, dealuminated. Figure 5 clearly shows that the amount of framework aluminum decreases in the process. Similarly, the nutation spectra of realuminated samples R-3 and R-4 demonstrate that the aluminum does go back into the framework. As realumination progresses, the F signal increases at the expense of the other signals.

7. NMR Studies of the Structure of Brønsted Acid Sites

The study of acidic surface sites capable of donating protons to adsorbed molecules is one of the most important in heterogeneous catalysis. It is vital to know the concentration, strength, and accessibility of the Brønsted and Lewis acid sites and the details of their interaction with the adsorbed organics. The Brønsted acidity of zeolites arises from the presence of accessible hydroxyl groups associated with framework aluminum ("structural hydroxyls"). Extensive ^{1}H MAS NMR measurements have led to the assignment of the various proton resonances as follows:[86,87]

Signal "a" at 1.3–2.3 ppm from tetramethylsilane (TMS), due to nonacidic (silanol) hydroxyls on the surface of zeolite crystallites and crystals defects sites

Signal "b" at 3.8–4.4 ppm from bridging OH groups involving O_1 oxygen atoms and pointing toward the zeolitic supercages

Signal "c" at ca. 5 ppm from protons on O_3 atoms and pointing toward the other oxygens in the sodalite cages

Signal "d" at 6.5–7.0 ppm, due to residual NH_4^+ cations

Signal "e" at 2.6–3.6 ppm, due to Al–OH groups attached to nonframework Al.

^{1}H NMR of static samples can readily probe the geometry of the Brønsted acid site.[88,89] It is a convenient tool for the determination of the Al–H distance, because the second moment of the broad-line proton spectra,

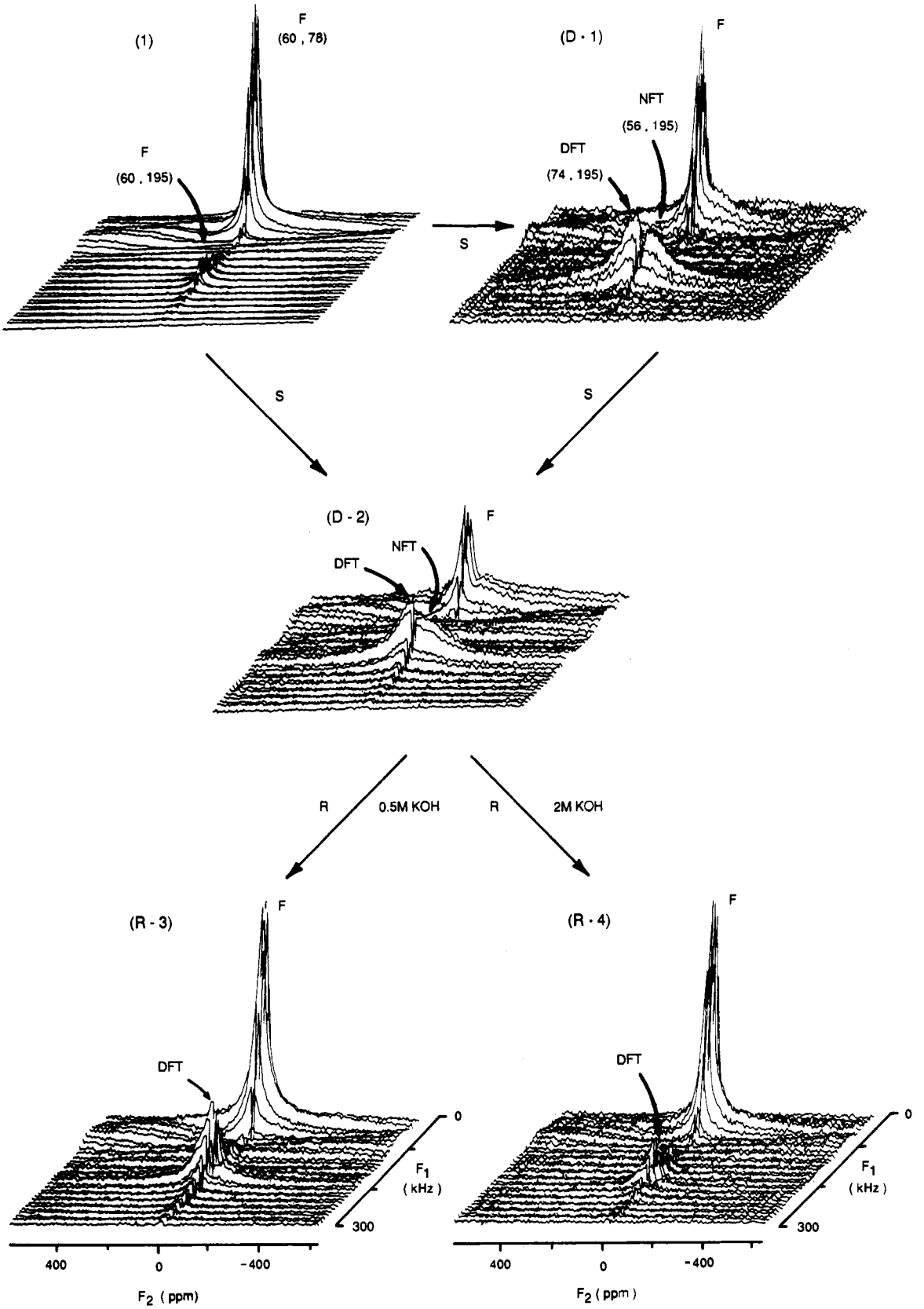

Figure 5. ^{27}Al quadrupole nutation spectra of hydrothermal dealumination/realumination.[79] Parent sample 1 (Si/Al ratio of 2.56) has been steamed (S) for various lengths of time to give dealuminated samples D-1 and D-2 (framework Si/Al ratios of 3.10 and 4.91). Sample D-2 has been realuminated (R) with KOH to give samples R-3 and R-4 (Si/Al ratios of 2.59 and 1.54).

which is inversely proportional to the *sixth* power of the distance between the dipole-coupled nuclei, is dominated by the ^{1}H–^{27}Al interaction. Spectra are obtained by the Fourier transformation of the FID following the $\pi/2 - \tau - \pi$ pulse sequence. An argument based on van Vleck's formula[90] can be used[91] to calculate the aluminum–proton distance, r_{Al-H}, from the second moment, M_2:

$$r_{Al-H} = \sqrt[6]{126.09/M_2} \quad (2)$$

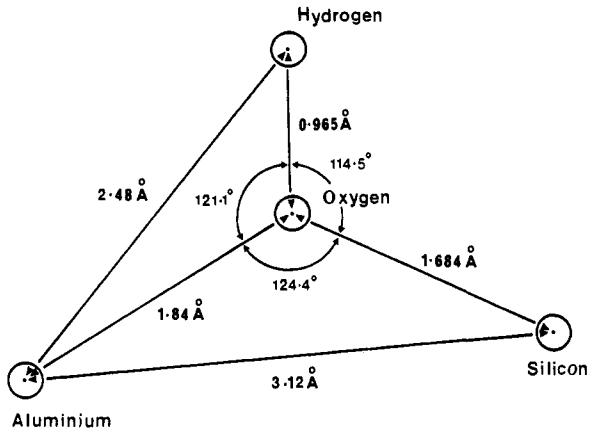

Figure 6. The geometry of the Brønsted acid site in zeolite H-ZSM-5.[88,89] Atomic radii are not to scale.

where r_{Al-H} is in Å and M_2 in units of 10^{-8} T^2. The conditions which must be met for this method to be quantitatively correct are:

(1) Dipole–dipole interactions additional to the interaction between a single proton and a *single* aluminum nucleus are either absent or taken into account;

(2) The nonresonant spins (e.g. ^{27}Al when observing ^1H) are oriented in the Zeeman field and not in the quadrupole field;[92]

(3) Line broadening due to chemical shift anisotropy is either negligible or taken into account;

(4) The protons are immobile and the apparent second moment is not motionally reduced.

^1H NMR studies of zeolite H-Y have concluded[88,89] that (i) the experimentally measured M_2 is 0.88×10^{-8} T^2; (ii) the interactions with other protons contribute 0.05×10^{-8} T^2; (iii) the mean total contribution of second-nearest Al atoms to M_2 of O_1 and O_3 hydroxyls is 0.06×10^{-8} T^2; (iv) the contribution of quadrupolar effects is negligible; (v) the anisotropy of the chemical shift contributes 0.08×10^{-8} T^2; and (vi) for the purpose of the second moment the zeolitic framework is rigid. Equation 2 shows that the final value $M_2 = 0.69 \times 10^{-8}$ T^2 for an isolated bridging hydroxyl group corresponds to $r_{H-Al} = 2.38 \pm 0.04$ Å.

In zeolite H-ZSM-5 the second moment arising from the interaction with other protons and second-nearest aluminum atoms is always negligible. The second moment attributable to SiOH groups on framework defects measured in the parent zeolite Na-ZSM-5 (which contains very few bridging hydroxyls) is $(0.40 \pm 0.2) \times 10^{-8}$ T^2. Considering that in H-ZSM-5 the SiOH groups amount to 20% of the total hydroxyl concentration, $M_2 = (0.54 \pm 0.04) \times 10^{-8}$ T^2 for bridging hydroxyl groups. The theoretical line shape of a ^1H–^{27}Al pair is a superimposition of *three* Pake doublets: one due to the interaction of ^1H with ^{27}Al in the states with $S = \pm^1/_2$ and two doublets due to $S = \pm^3/_2$ and $S = \pm^5/_2$. The second moment calculated from the distance between the $\pm^5/_2$ singularities found in the spectrum gave $M_2 = (0.54 \pm 0.05) \times 10^{-8}$ T^2, which corresponds to $r_{H-Al} = 2.48 \pm 0.04$ Å for the bridging hydroxyl groups. The structure of the active site in zeolite H-ZSM-5 is shown in Figure 6. The Al–H distance is larger than in zeolite H-Y because of the smaller T–O–T angles in a framework composed mostly of 5-membered rings.

Vega and Luz[93] characterized zeolite NH_4-rho and vacuum-calcined H-rho by multinuclear NMR. They were able to propose a two-step calcination procedure for the preparation of H-rho. The anhydrous product has ca. 11 hydrogen atoms per unit cell in Brønsted acid sites, some rigid and some undergoing fast large-amplitude librations. No translational diffusion between different sites was observed.

Batamack et al.[94] carried out a broad-line and high-resolution NMR studies of the hydroxonium ion in zeolite H-ZSM-5. Line-shape simulation of the ^1H NMR signal measured at 4 K shows that for water concentrations about equal to the concentration of bridging hydroxyl groups in defect-free zeolite two configurations exist: water molecules hydrogen bonded to the bridging OH group and the hydroxonium ion.

Scholle et al.[95,96] used ^1H MAS NMR to study the acidity of the hydroxyl groups in zeolite H-ZSM-5 and its borosilicate "equivalent", known as H-boralite, at various water contents. They were able to distinguish terminal and water hydroxyls from acidic hydroxyl groups in the framework. H-ZSM-5 was found to be more acidic than H-boralite.

There is at present only a handful of publications involving ^{15}N NMR of molecules sorbed on zeolites, but they establish beyond doubt the power of the technique for the study of zeolitic acidity and other surface phenomena. The nitrogen atom in molecules such as ammonia and pyridine has a lone pair of electrons and binds directly to the surface site. One is therefore observing large effects on a nucleus with a wide (ca. 900 ppm) range of chemical shifts, rather than more indirect influence as in the case of ^{13}C. Michel et al.[97,98] and Jünger et al.[99] measured the spectra of isotopically enriched ammonia, trimethylamine, pyridine, and acetonitrile on various zeolites at 9.12 MHz and found that resonance shifts depended strongly on the interactions of sorbate molecules with cations and Brønsted and Lewis acid sites. The ^{15}N chemical shift changes by 18.5 ppm as the pore-filling factor Θ of $^{15}NH_3$ on zeolites Na-X, Na-Y, Na-mordenite, and Na-Y varies between 0 and 1. In sodium forms, the resonance shift is mainly due to intermolecular interactions. For ultrastable zeolite Y, the ^{15}N resonance of ammonia does not change between $\Theta = 0.2$ and 0.72, and is approximately equal to that measured for liquid ammonia (18 ppm from nitromethane). Michel et al.[97,98] concluded that at higher Θ the ammonia molecules are packed so closely that their resonance shift becomes liquid like. In ultrastabilized samples strong association of ammonia molecules occurs even at low coverages leading to constant chemical shift. At low coverages, the resonance shift of $^{15}NH_3$ on zeolite H-Y remains constant and is close to that for NH_4^+ solutions, which shows that all ammonia molecules are converted into ammonium cations as a consequence of interaction with structural hydroxyl groups. Consideration of the equilibrium between the surface sites and the sorbate allows the resonance shifts for the surface complexes to be obtained and to eliminate the influence of the exchange process. The formation of pyridinium ions in ultrastable zeolites has been followed, leading to direct determination of the number of interacting hydroxyl groups. ^{15}N is far superior to ^{13}C for this purpose. Acetonitrile can be conveniently used for characterization of interactions with the exchangeable cations and Lewis acid sites.[97–99] Electron-acceptor strength of

ultrastable zeolites increases with the increased temperature of activation, the rise being particularly drastic in the region 300–400 °C. NMR shows unambiguously that the exchangeable cations in zeolite X act as adsorption centers.

Trimethylphosphine has also been used[100,101] as a probe in ^{31}P MAS NMR studies of zeolite H-Y. When a sample is activated at 400 °C, the spectrum is dominated by the resonance due to $(CH_3)_3PH^+$ complexes formed by chemisorption of the probe molecule on Brønsted acid sites. At least two types of such complexes were detected an immobilized complex coordinated to hydroxyl protons and a highly mobile one which is desorbed at 300 °C.

8. Chemical Status of Guest Organics in the Intracrystalline Space

The declining oil reserves have stimulated considerable efforts toward the exploration of alternative sources of energy and organic chemicals. One solution is to use the abundant supply of coal as a source of synthesis gas ($CO + H_2$) which is readily converted to methanol (MeOH). MeOH can then be transformed into higher molecular weight hydrocarbons (olefins, aliphatics and aromatics) over shape-selective zeolite catalysts, the most successful of which in this respect is H-ZSM-5, capable of converting MeOH to hydrocarbons up to C_{10}. The selective synthesis of ethylene and propylene, the key intermediates for the production of detergents, plasticizers, lubricants and a variety of chemicals, proceeds over smaller pore zeolites such as chabazite and erionite.

The transformation of methanol to hydrocarbons over zeolite H-ZSM-5 is the basis of several industrially important reactions, such as the MTG or the MTO processes.[102,103] The mechanism of the reaction, particularly as concerns the formation of the first C–C bond and the nature of the interactions between the CH_3OH molecules and the zeolitic framework has been the subject of controversy.[104,105] ^1H NMR has been used[106–108] to study the chemistry of methanol adsorbed on H-ZSM-5.

In MAS NMR experiments[107,108] samples were contained inside capsules[109] which could be spun inside the MAS NMR probehead at rates of up to 3 kHz. The design of the capsule allowed the samples to be dehydrated at 400 °C under a pressure of 10^{-5} mbar before adsorption of the organic. Capsules were then sealed while keeping the sample at liquid nitrogen temperature in order to prevent the onset of chemical reactions. High-resolution ^1H MAS NMR spectra were recorded using 2 μs (20°) pulses with a repetition time of 5 s. Since the ^1H spin–lattice relaxation times of adsorbed alcohols on zeolites were found to be of the order of 0.2 s, such repetition times generate quantitatively reliable spectra.

Hydrogen bonding causes a downfield chemical shifts in alcohols because of the deshielding of the proton as a result of electrostatic polarization of the OH bond. In liquid CH_3OH hydrogen bonding causes a downfield shift of 3.1 ppm (Figure 7b) relative to CH_3OH in CCl_3D where there is no hydrogen bonding (Figure 7c). The proton MAS NMR spectrum of CH_3OH adsorbed on zeolite H-ZSM-5 (Figure 8a) contains a signal at 4.1 ppm corresponding to the methyl protons and another

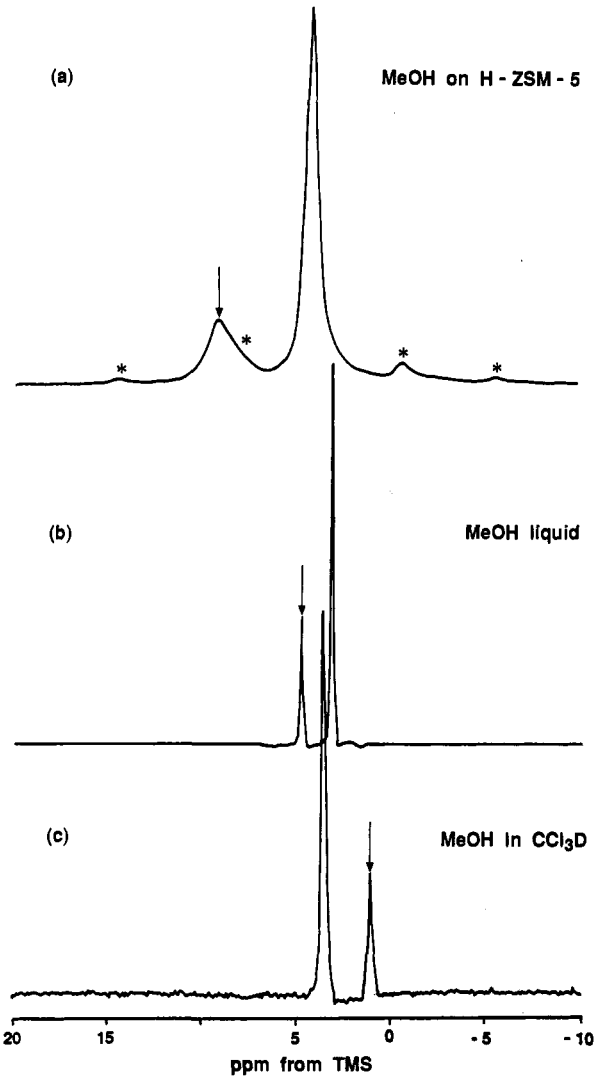

Figure 7. ^1H MAS NMR spectra[108] of (a) CH_3OH adsorbed on zeolite H-ZSM-5; (b) neat liquid CH_3OH; (c) CH_3OH dissolved in $CDCl_3$. Asterisks denote spinning sidebands, arrows point to the position of the resonance from the methanol hydroxyl.

at 9.1 ppm corresponding to the hydroxyl protons. When CD_3OH is adsorbed only the 9.1-ppm signal is observed, which demonstrates that all hydroxyls resonate at the same chemical shift. When 6 molecules of CD_3OH are adsorbed per Brønsted site on zeolite H-ZSM-5 (Figure 8a) one signal corresponding to the hydroxyl groups is found at 9.1 ppm. By contrast, when CH_3OD is adsorbed (Figure 8b), apart from the signal at 4.1 ppm corresponding to the methyl groups there is a small resonance at ca. 9.4 ppm. Adsorption of CD_3OD demonstrates that this latter signal originates initially from the framework Brønsted acid sites and not from the methyl group (Figure 8c). The low-intensity signals at 0–2 ppm are due to the probehead background. This was checked by repeating the experiments under identical conditions with the sample removed.

The large downfield shift of the hydroxyl resonance of the CH_3OH upon adsorption on H-ZMS-5 must be caused by very strong hydrogen bonding and/or direct protonation of the alcohol. Note that all hydroxyl groups in the spectrum given in Figure 8 resonate at the same chemical shift, which indicates that all protons should be equivalent on the time scale of the NMR

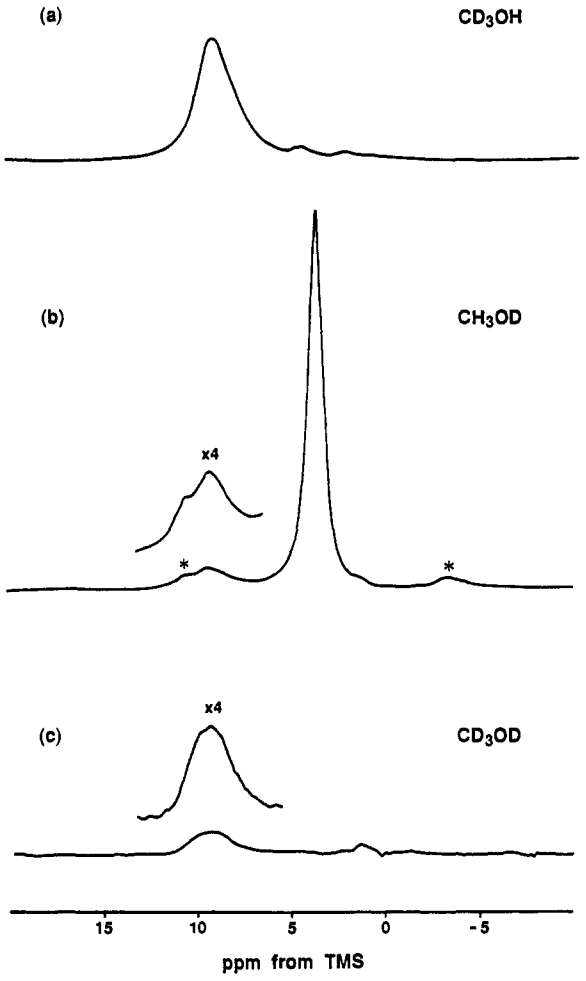

Figure 8. ^1H MAS NMR spectra[108] of (a) CD_3OH adsorbed on H-ZSM-5; (b) CH_3OD adsorbed on H-ZSM-5; (c) CD_3OD adsorbed on H-ZSM-5. Asterisks denote spinning sidebands.

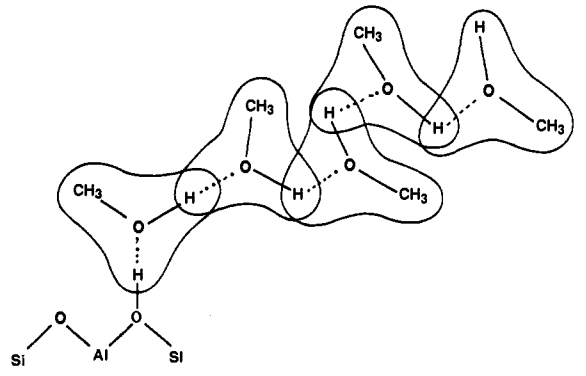

Figure 9. Protonated cluster of hydrogen bonded methanol molecules at the Brønsted acid site.[108]

experiment. Consider the scheme shown in Figure 9, which involves a hydroxyl proton protonating five methanol molecules. It is clear that, in this resonance structure, each molecule of methanol is formally identical to a methoxonium ion. The charged cluster, a supercation, may rotate in the intracrystalline space so that different hydroxyl protons approach the bridging framework oxygen in turn, thus becoming equivalent on the NMR time scale.

At the lower coverage of 2 molecules per Brønsted acid site, the hydroxyl signal moves from 9.1 ppm in Figure 8a to 10.5 ppm. This experiment indicates the presence of fast exchange between the proton of the zeolitic acid site and the OD group of the adsorbed methanol.

The downfield shift of the hydroxyl resonance of MeOH is a good measure of the proton donating ability of the solid acid catalyst. In zeolites H-Y and H-L the shifts are considerably smaller than in H-ZSM-5, which is consistent with their lower acidity. The advantage of our MeOH adsorption method for the measurement of catalytic activity is that it monitors the species to which the proton is donated (the MeOH molecule) rather than the Brønsted acid site.

It is interesting to note that the chemical shift of the hydroxyl resonance is very sensitive to the type of zeolite on which methanol is adsorbed.[108] The change in the hydroxyl chemical shift in H-ZSM-5 is by far the largest (7.8 ppm downfield from $MeOH/CCl_3D$). The position of this resonance also depends on the method of synthesis of ZSM-5. When a zeolite with almost the same Si/Al ratio is prepared using the low-pH "fluoride" route, the corresponding increase of chemical shift is only 6.0 ppm. This result is intriguing. In terms of Si/Al ratio the zeolites are identical. The major difference is the lack of defect sites in the material synthesized via the fluoride method. This hints that defect sites such as SiOH nests might also be responsible for the extraordinary hydrogen-bonding properties of conventionally prepared H-ZSM-5.

The sodium form of the zeolites shows only very small shifts in the hydroxyl resonance upon adsorption of MeOH. In the case of Na-ZSM-5 the shift is in fact over 1 ppm *upfield* from liquid MeOH (increased shielding of the proton or less hydrogen bonding). This can be explained in terms of coordination of the MeOH to the coordinatively unsaturated sodium cations via the MeOH oxygens, which in effect breaks up the bonding present in the liquid phase. In the series Na-ZSM-5, Na-Y, Na-A there is a progressive increase in the downfield shift of the hydroxyl resonance. This is most easily explained in terms of the increase in Al content of the zeolite framework which increases the total electrostatic charge of the framework oxygen. Consequently, this provides a greater opportunity for hydrogen bonding of methanol to the zeolite framework adjacent to an aluminum atom in zeolites A or Y.

^{13}C MAS NMR is useful for the elucidation of the nature of the interaction of methanol with zeolitic and silicoaluminophosphate-based molecular sieves prior to the onset of catalytic reactions. *Slow* magic-angle spinning ^{13}C NMR reveals[100] that strongly bound surface CH_3–O–Si groups are formed at 250 °C when methanol is adsorbed on the molecular sieve SAPO-5. Figure 10a shows the ^{13}C MAS NMR spectrum of methanol (MeOH) adsorbed on SAPO-5 at room temperature and not subsequently heated. A single sharp resonance is observed at 50 ppm corresponding to relatively highly mobile adsorbed methanol. After the sample was heated to 150 °C for 10 min 37% of the MeOH has been converted to dimethyl ether (DME) which, judging from its narrow spectral line (Figure 10b), is also highly mobile. Further heating to 250 °C for an additional 10 min results in the spectrum shown in Figure 10c. Although a number of broad spectral features are in evidence, they all correspond to two chemical species, one at 50 ppm corresponding to methanol and a broader signal at 60 ppm with associ-

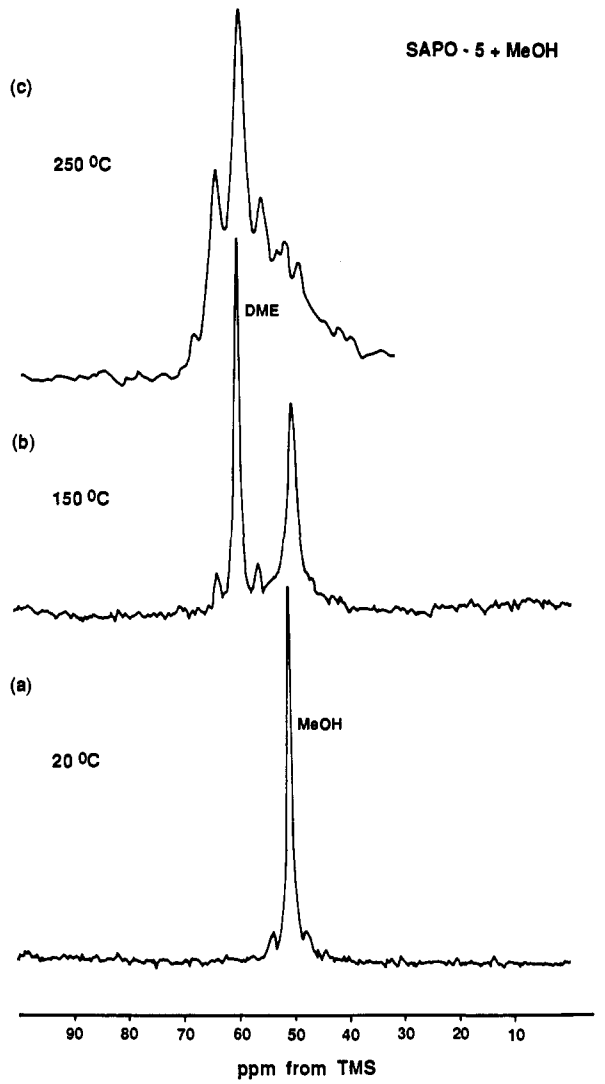

Figure 10. ^{13}C MAS NMR spectra of methanol adsorbed on SAPO-5:[110] (a) room temperature spectrum; (b) spectrum of a sample heated to 150 °C for 10 min; (c) sample heated to 250 °C for 10 min.

ated spinning sidebands. The greatly increased linewidth of the latter species together with the presence of sidebands in this typical solid-state spectrum indicate the presence of considerable chemical shift anisotropy resulting from much reduced molecular mobility. The MAS spinning frequency used for these experiments was below 1 kHz. It is clear that the application of normal, much higher, spinning frequencies would average this anisotropy thus concealing important chemical information.

The likely origin of the broad new signal are the strongly bound surface CH_3–O–Si methoxy groups which would have a very similar chemical shift to that of DME. Being anchored at the surface of an aluminum-rich molecular sieve, these methoxy groups undergo both chemical shift and dipole–quadrupole broadening effects brought about by the vicinity of ^{27}Al nuclei. After subsequent heating of the sample to 300 °C and above methanol is converted to a mixture of mobile olefins and aliphatics which can be observed with slow MAS and which give narrow spectral lines without spinning sidebands. This demonstrates the progression from a weakly bound methanol molecule to a strongly bound reaction intermediate and finally to a weakly bound hydrocarbon product. By contrast, in zeolite H-ZSM-5 methanol becomes strongly bound to the framework at room temperature without the formation of methoxy groups.[110]

9. *In Situ Studies of Catalytic Reactions on Molecular Sieves*

The catalytic conversion of methanol to hydrocarbons in the gasoline boiling range using zeolite ZSM-5 at ca. 370 °C has understandably attracted much attention. ^{13}C MAS NMR can probe directly the role of the active site in shape-selective catalytic reactions on zeolites in situ. The kind and quantity of chemical species present inside the particle can now be directly monitored.[111-118] This information, not forthcoming from other techniques, is usefully compared with the composition of the gaseous products to give new insights into reaction pathways on molecular sieves and to assist in the design of new shape-selective catalysts. These experiments have (i) identified 29 different organic species *in the adsorbed phase* and monitored their fate during the course of the reaction, (ii) observed directly different kinds of shape selectivity in a zeolite, and (iii) unequivocally distinguished between mobile and attached species. The results will assist in the design of shape-selective solids and provide a better understanding of catalytic processes in the intracrystalline space.

Shape selectivity of zeolites[3,120-123] arises from the fact that the probabilities of forming various products in the narrow intracrystalline cavities and channels are largely determined by molecular dimension and configuration. Three kinds of shape selectivity have been envisaged.[3] "Reactant selectivity" occurs when only certain molecules can access the intracrystalline space and react there, others being too large to enter the pores. In "product selectivity" only some of the various species formed within the channels and cavities can diffuse out of the crystalline and appear as reaction products. "Restricted transition-state selectivity" takes place when certain reactions cannot proceed at all because they would involve transition states requiring more space than is available in the intracrystalline space. The evidence for the existence of the product and transition-state selectivities available so far is indirect since it relies on the *absence* of certain species in the products rather than on the *presence* of others in the intracrystalline space, something which has not until now been directly monitored.

^{13}C MAS NMR of sealed H-ZSM-5 samples gives a considerable gain in resolution in comparison with earlier work.[124-130] The spectrum of a sample with adsorbed MeOH and maintained at 20 °C (Figure 11a), contains a single resonance at 50.8 ppm due to MeOH. After heating the sample to 150 °C for 20 mins the spectrum (Figure 11b) is composed of two signals, at 50.5 and 60.5 ppm, corresponding to MeOH and DME, respectively.

Figure 12 shows the spectrum of a sample treated at 300 °C for 35 min. MeOH and DME have been completely converted to a mixture of aliphatics and aromatics. The question arises as to how the various ^{13}C resonances are to be assigned to different hydrocarbon species, although some of them, especially those from methyl groups attached to aromatic rings, overlap. It turns out that all signals can be reliably assigned.[131-133]

TABLE I. Parameters of the Two-Dimensional Spectrum Shown in Figure 13

signal	chemical shift, ppm	signal multiplicity	J-coupling, Hz	tentative assignment[112]	final assignment
a	24.7	4	135	isobutane	isobutane
b	22.2	4	135	n-hexane isopentane n-heptane	isopentane
c	18.7	4	135	methyl-substituted benzenes	methyl-substituted benzenes
d	16.7	3	130	propane	propane
	16.0	4	130		
e	−11.0	5	135	methane	methane

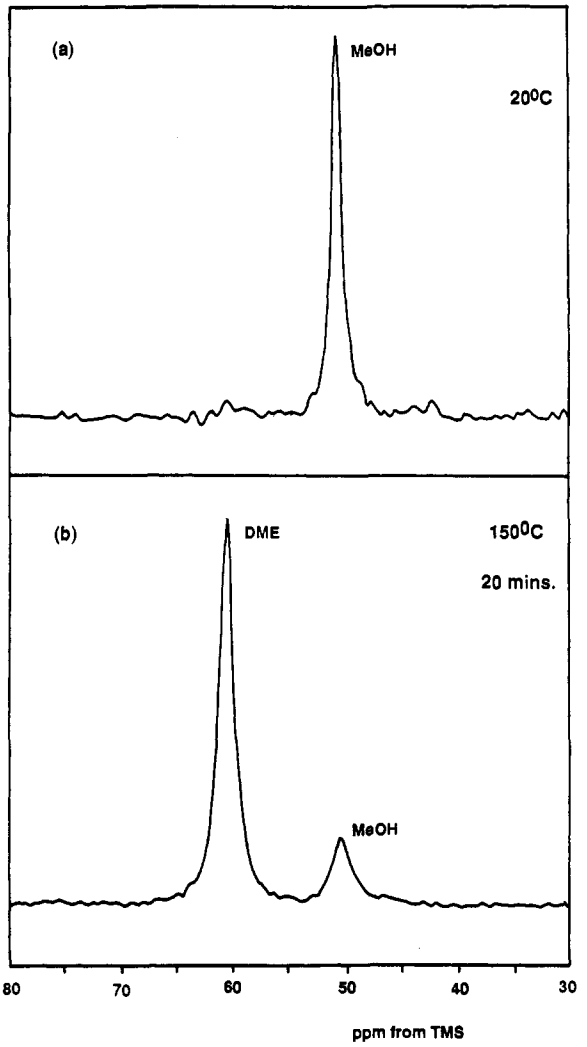

Figure 11. ^{13}C MAS NMR spectra of H-ZSM-5 with 50 Torr of adsorbed MeOH and recorded at room temperature:[112] a no heating and b 150 °C for 20 min. Experiments were performed at room temperature. High-power decoupling (but no cross-polarization) was used with 40° ^{13}C pulses and a 10-s repetition time. Asterisks denote spinning sidebands.

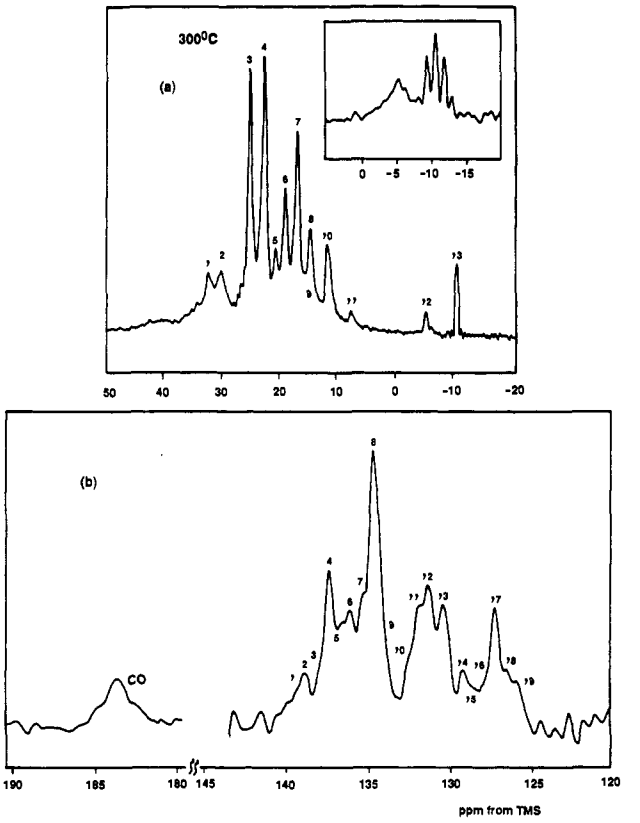

Figure 12. ^{13}C MAS NMR spectra of a sample heated to 300 °C for 35 min and recorded with proton decoupling only (a) aliphatic region and (b) aromatic and CO region.[112] Intensities in a and b are not on the same scale. The inset shows J-coupling of methane and cyclopropane carbons (recorded without decoupling). Spectral assignments are as follows: [peak numbers and intensities (s = strong, m = medium, w = weak) are in brackets, { } for aliphatic and ( ) for aromatic]: isobutane {3, s}; propane {7, s}; n-butane {3, 9, m}; n-hexane {1, 4, 8, m}; isopentane {1, 2, 4, 10, m}; n-heptane {1, 2, 4, 8, m}; methane {13, m}; ethane {11, w}; cyclopropane {12, w}; o-xylene (4, 12, 17, s){5}; p-xylene (7, 13, s){6}; m-xylene (2, 12, 15, 17, w){5}; toluene (2, 13, 14, 18, 2){5}; 1,2,4-trimethylbenzene (4,6,8,11,13,16, m){5, 6}; 1,3,5-trimethylbenzene (3, 16, w){5}; 1,2,3-trimethylbenzene (5, 7, 16, 19, w){5, 8}; 1,2,4,5-tetramethylbenzene (8, 11, s){6}; 1,2,3,5-tetramethylbenzene (5, 7, 10, 13, m){5,8}; 1,2,3,4-tetramethylbenzene (7, 9, 16, w){5, 8}. Because of the different Overhauser enhancements of different carbons, peak intensities give only an approximate concentration of the various species.

First, note that most compounds give rise to several NMR peaks. In addition to chemical shift information, and the monitoring of the number and relative intensity of the various ^{13}C signals, two-dimensional ^{13}C spectra have been used[132,133] to determine the connectivity of carbons and the number of protons attached to each carbon atom in the various organics and the details of ^{13}C–^{1}H couplings, enabling firm assignments for a number of resonances to be made.

A well-resolved two-dimensional J-coupled spectrum,[132] measured using no decoupling during part of the evolution period while synchronizing the time increment and the rotation period of the MAS spinner, is given in Figure 13 (Table I). The relative intensities of the $N + 1$ lines in a spectrum of a spin $^1/_2$ nucleus coupled to N equivalent spin $^1/_2$ nuclei are given by Pascal's triangle as 1:1 for $N = 1$; 1:2:1 for $N = 2$; 1:3:3:1 for $N = 3$; and 1:4:6:4:1 for $N = 4$. Multiplicities of the lines confirm that our assignments, based on conven-

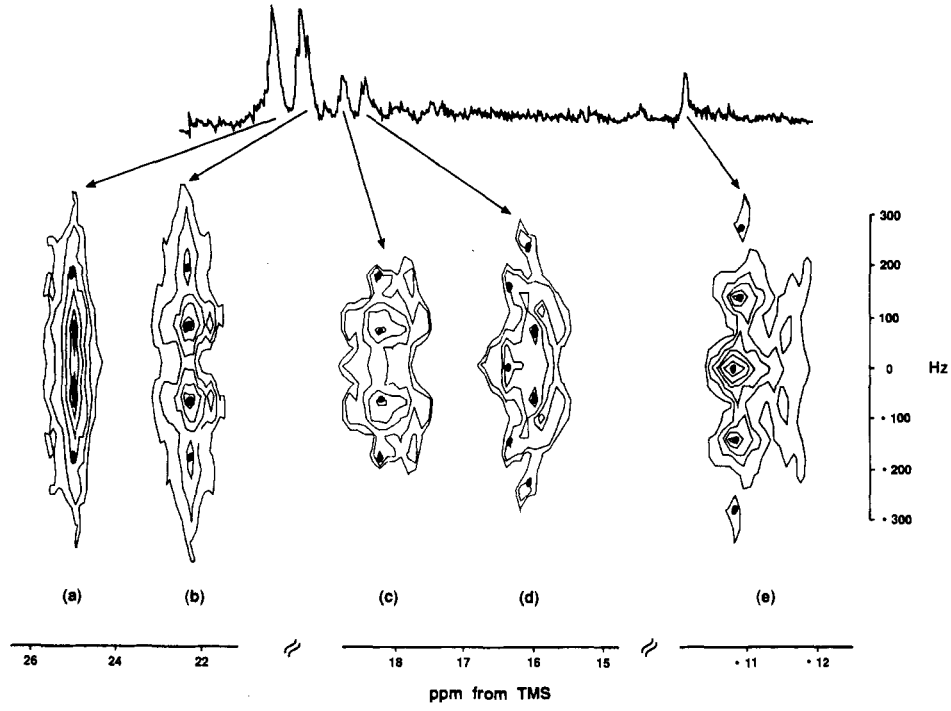

Figure 13. Heteronuclear two-dimensional J-resolved ^{13}C MAS NMR spectrum of zeolite H-ZSM-5 with adsorbed methanol treated at 300 °C for 30 min.[132]

tional one-dimensional spectra, are correct. For example, the resonance at −10.7 ppm in Figure 13 is split into 5 components with a requisite intensity ratio in the 2-D spectrum, which confirms that it must be due to adsorbed methane. Similarly, the 4-fold (methyl) and 3-fold (methylene) signals clearly indicate the presence of propane adsorbed in the intracrystalline space.

The 2D spin diffusion ^{13}C NMR experiment allows us to examine further the spectral assignments obtained from the 1D and the 2D J-resolved experiments.[133] It also provides new details concerning distribution of hydrocarbons in zeolite ZSM-5. Spectral spin diffusion in the solid state involves simultaneous flip–flop transitions of dipolar-coupled spins with different resonance frequencies. The interaction of the X nuclei undergoing spin diffusion with the proton reservoir provides compensation for the energy imbalance. Spin diffusion results in an exchange of magnetization between nuclei responsible for resolved NMR signals, which can be conveniently detected by observing the relevant cross-peaks in the 2D spin-diffusion spectrum. The technique is well established for solids. The rate of spin diffusion is very strongly dependent on the internuclear separation r, being proportional to $1/r^3$ for a rigid crystal lattice and to $1/r^6$ for species undergoing rapid isotropic motion. As a result, for all practical purposes spin diffusion occurs only between nuclei in adjacent functional groups within the same molecule (the intramolecular case) or between nuclei in neighboring molecules mixed on a microscopic level (the intermolecular case). Both cases are observed in our system.

Figure 14 shows the 2D spin-diffusion spectrum of aliphatic hydrocarbons trapped in the zeolite. The 1D signals, corresponding to the diagonal peaks in the 2D spectrum, have been assigned previously,[111-112] but the assignment of signal b has subsequently been questioned.[132] It is clear that n-hexane and n-heptane are present, since signal e comes exclusively from their CH_3

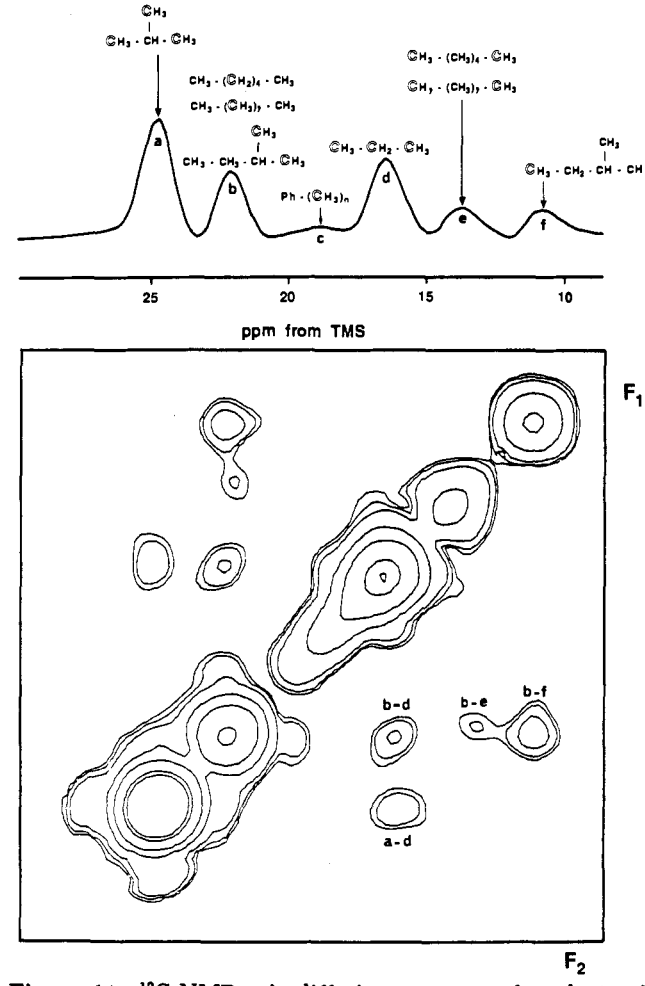

Figure 14. ^{13}C NMR spin diffusion spectrum of products of methanol conversion into gasoline over zeolite ZSM-5 with the projection onto the F_2 axis (corresponding to a conventional spectrum) at the top.[133] Carbon atoms to which individual resonances are assigned are highlighted. For signal assignment see Table II.

TABLE II. Assignment of the 2D ^{13}C NMR Spin-Diffusion Spectrum in Figure 14.

Diagonal Peaks

signal	chemical shift, ppm	group	assignment
a	24.7	CH_3	isobutane
b	22.3	$CH_3CH_2CH(CH_3)_2$	isopentane
		CH_2	*n*-hexane + *n*-heptane
c	18.7	CH_3	methyl-substituted benzenes
d	16.7	$CH_3 + CH_2$	propane
e	14.3	CH_3	*n*-hexane + *n*-heptane
f	11.2	$CH_3CH_2CH(CH_3)_2$	isopentane

Cross-Peaks

signals	assignment	type of spin diffusion
a–d	isobutane–propane	intermolecular
b–d	isopentane–propane	intermolecular
b–e	*n*-hexane	intramolecular
	n-heptane	intramolecular
b–f	isopentane	intramolecular

groups. Therefore, considering the chemical shift of CH_2 groups of *n*-hexane and *n*-heptane, both hydrocarbons must contribute to signal b. In the *J*-resolved experiment this signal was not split into a triplet, because no homonuclear proton decoupling was applied during the first half of the evolution period, so that the splitting was obscured by substantial dipolar broadening. By contrast, CH_3 groups of isobutane undergo free rotation, which reduces the dipolar interaction and allows the quartet splitting of signal b to be observed. We note that signals of *n*-butane in the spin-diffusion spectrum are missing, since cross-polarization has a tendency to underestimate signals of mobile products, so that only those which are as abundant as propane appear.

Zeolite ZSM-5 contains no cages and its channel diameter only allows the hydrocarbon species in the channels to be lined up sequentially. For any two molecules to exchange their positions, access to an unoccupied channel crossing is required, which is difficult to satisfy at high adsorbate loadings. Hydrocarbon molecules are only capable of limited motion along the channels, which does not favor *intermolecular* spin diffusion. Free molecular rotation cannot occur, so that *intramolecular* dipolar interactions are present even for quite mobile functional groups and make the intramolecular spin diffusion possible. Thus intramolecular spin diffusion in our system is preferred to intermolecular spin diffusion. The assignments of the various signals are given in Table II.

Munson et al.[117] questioned the suggestion in refs 111 and 112 that, since CO is observed prior to hydrocarbon formation, it is an intermediate in the reaction. Methanol-^{13}C and formic acid-^{13}C were first coadsorbed on the H-ZSM-5 catalyst, and an in situ NMR experiment was performed. It was found that the conversion rate of methanol was not affected by large quantities of CO. The authors then measured the spectra of a sample containing formic acid-^{13}C and unlabeled methanol. ^{13}CO was not incorporated in the reaction product. The conclusion is that CO is neither an intermediate nor a catalyst in MTG chemistry.

Aronson et al.[134] used ^{13}C NMR to identify the intermediates formed upon the adsorption of 2-methyl-2-propanol on zeolite H-ZSM-5. The adsorbed species can best be described as a highly reactive silyl ether, with the alkyl group covalently bonded to oxygen of the zeolitic framework. They assign the signal at 77 ppm to the carbon bonded to the oxygen, and the signal at 29 ppm as due to aliphatic carbons formed in secondary reactions. Richardson et al.[113] studied the mechanisms by which butadiene oligomerizes in acidic zeolitic catalysts. It was found that oligomerization proceeds primarily by 1,4-addition and that secondary reactions of the oligomers are strongly dependent upon the properties of the zeolite. Thus the initially formed product undergoes cyclization to form fused rings in zeolite H-Y, but isolated rings are formed in the smaller channels of zeolite H-ZSM-5. These results provide insight into the mechanisms by which oxide catalysts are deactivated by pore blockage. The conclusions of Anderson et al.[118] are in agreement with the steric arguments given by the Texas group. They used ^{13}C and ^{1}H MAS NMR to monitor the formation of long-chain polymeric hydrocarbons within the intracrystalline space of offretite during the conversion of methanol. The presence of such polymers was attributed to the uninterrupted one-dimensional pore system. In erionite, where the channel system is constricted at every 15 Å, polymers cannot form. It appears that a degree of channel "tortuosity" is preferable in reactions which produce readily oligomerizable molecules, in order to prevent undesirable side reactions.

The oligomerization of propene on zeolite H-Y has been studied[115,119] by variable-temperature ^{13}C MAS NMR. Alkoxy species formed between protonated alkenes and oxygens of the zeolitic framework were found to be important long-lived intermediates in these reactions. Simple secondary or tertiary carbocations are either absent in the zeolite at low temperatures or are so transient as to be undetectable by NMR even at temperatures as low as 163 K. There was, however, evidence for long-lived alkyl-substituted cyclopentenyl carbocations, which are formed as free ions in the zeolite at room temperature. At 503 K the oligomers crack to form branched butanes, pentanes, and other alkanes. The final product was highly aromatic coke. The structure, dynamics, and reactivity of an alkoxy intermediate formed from acetylene on zeolite catalysts have been investigated by Lazo et al.[114]

10. Direct Observation of Shape Selectivity

The *distribution* of adsorbed species in the sample of zeolite with adsorbed methanol treated at 300 °C is very different from that observed in the reaction products.[111,112] The principal aromatics expected to be present are *m*- and *p*-xylene, 1,2,4-trimethylbenzene, and toluene. However, the main species actually found in the adsorbed phase are *o*- and *p*-xylene and 1,2,4,5-tetramethylbenzene, with smaller amounts of 1,2,4-trimethylbenzene and 1,2,3,5-tetramethylbenzene. The other xylenes, tri- and tetramethylbenzenes are also found but in smaller amounts. The distribution of the three trimethylbenzenes in the adsorbed phases is very different from the thermodynamic equilibrium distribution (see Figure 15). The fact that 1,2,3- or 1,3,5-trimethylbenzenes (with kinetic diameters of 6.4 and 6.7 Å, respectively) are not found among the products, but are present in the adsorbed phase, while the smaller 1,2,4-trimethylbenzene (6.1 Å) is found in both, clearly demonstrates the reality of the concept of product selectivity. The channel dimensions of ZSM-5 are 5.6 ×

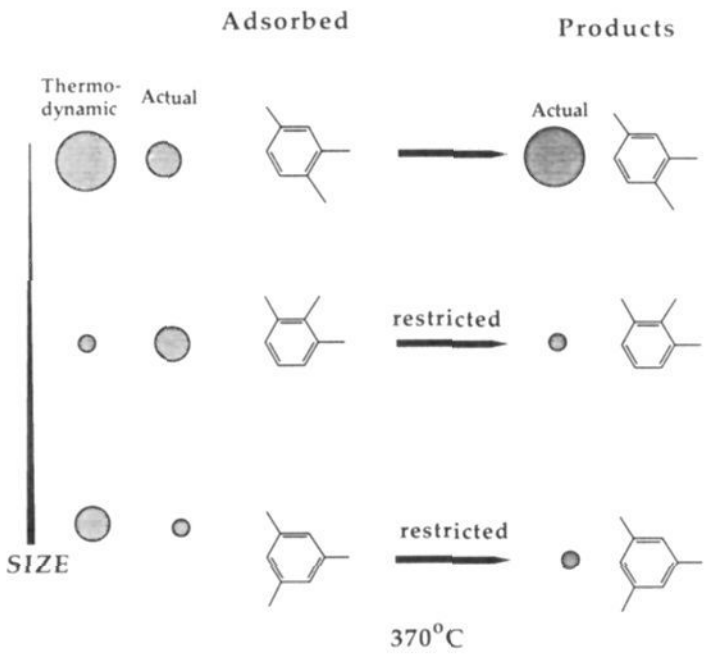

Figure 15. Schematic representation of the expected and actual distribution of the three trimethylbenzenes in the intracrystalline space and in the gaseous products of the reaction. Diameters of the circles are proportional to the intracrystalline content of each compound; the effective molecular size increases from top to bottom of the figure.

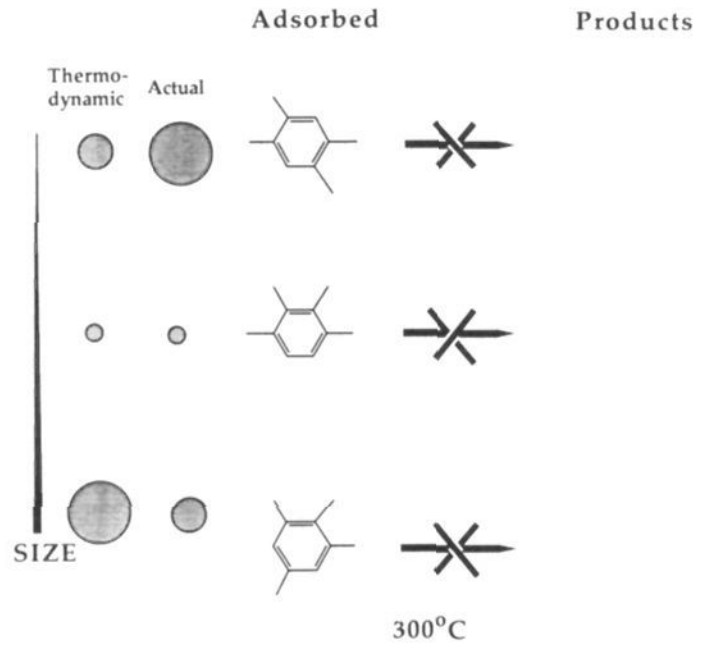

Figure 16. Schematic representation of the expected and actual distribution of the three tetramethylbenzenes in the intracrystalline space and in the gaseous products of the reaction. Diameters of the circles are proportional to the intracrystalline content of each compound; the effective molecular size increases from top to bottom of the figure.

5.3 Å, but more space is availale at the intersection of the straight and zigzag channels. While the greater amplitude of thermal vibrations of the framework, which increases the maximum effective size of the channels, allows the smaller isomer to diffuse out of the crystal, the two larger isomers, although formed, are unable to diffuse out at 300 °C and must isomerize to 1,2,4-trimethylbenzene.

The distribution of the tetramethylbenzenes in the intracrystalline space is most unexpected (see Figure 16). None of them have ever been reported in the products of the reaction at 300 °C and yet all three are clearly present in the adsorbed phase. Because of the restricted intracrystalline space they can only form at channel intersections, but (unlike the trimethylbenzenes) are not generated in the thermodynamic equilibrium distribution. 1,2,3,5-Tetramethylbenzene (6.7 Å) should be the dominent species on thermodynamic grounds; in fact it is 1,2,4,5-tetramethylbenzene

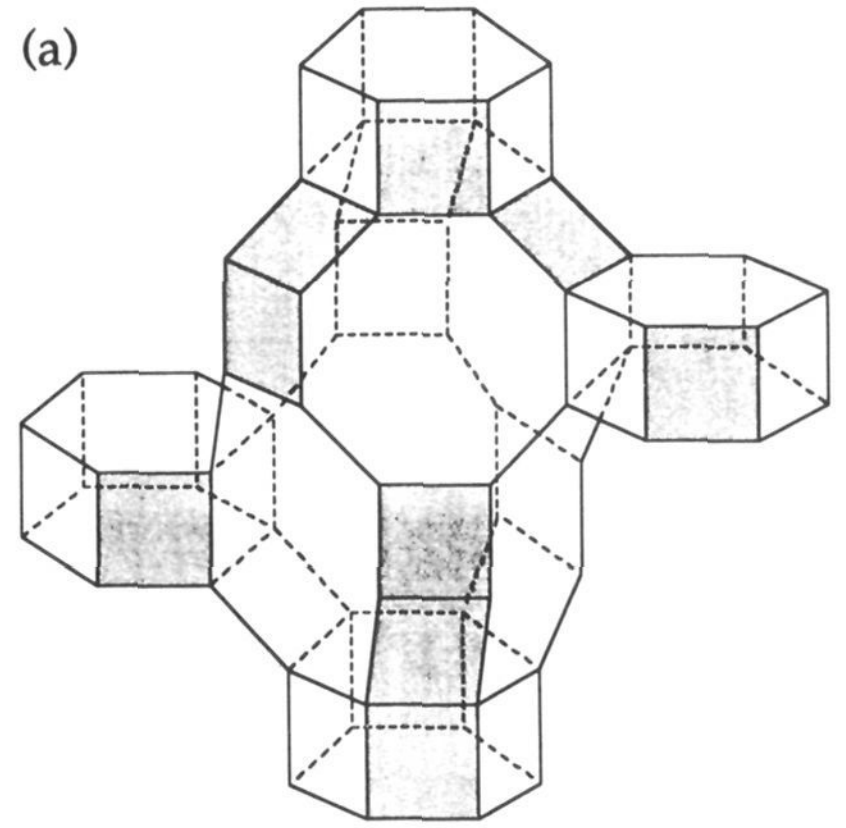

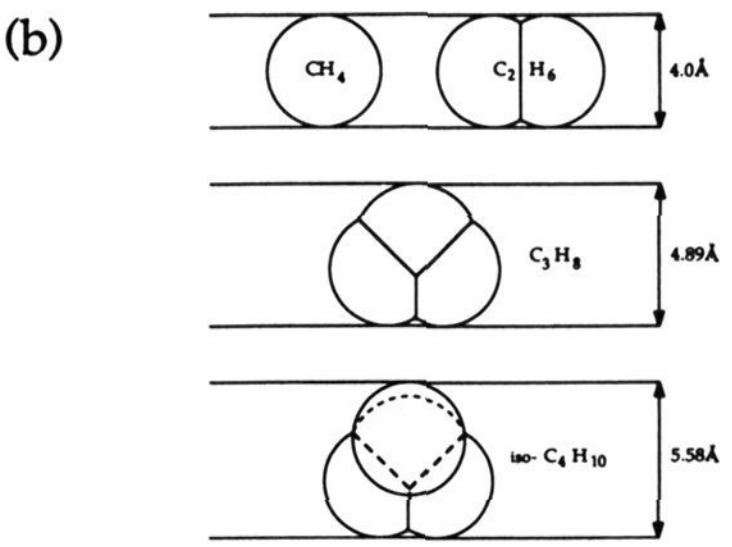

Figure 17. (a) The structure of SAPO-34/chabazite. (b) Kinetic diameters of relevant aliphatic molecules.[135]

(6.1 Å) which dominates. The thermodynamically least favored isomer, 1,2,3,4-tetramethylbenzene (6.4 Å), is found in small quantities. The fact that tetramethylbenzenes are not found in the products again demonstrates product shape selectivity. Their *relative abundance* in the adsorbed phase, on the other hand, shows that an additional kind of shape selectivity occurs within the intracrystalline space. It does not rely on the ability of species to enter or to leave the crystal nor on the size of the transition state: isomerization is sterically restricted within the crystalline at the active site itself.

It is instructive to compare the shape-selective catalytic conversion of methanol to low molecular weight olefins and aliphatics zeolite ZSM-5 with the results for the molecular sieve SAPO-34.[135] The sieve, which has the framework topology of the natural zeolite chabazite[136,137] (see Figure 17) is known to convert MeOH to hydrocarbons with a selectivity for C_2 of 33.8 mol %. In what follows, we shall refer to the gas species leaving the catalyst (and monitored by gas chromatography) as "products" and the compounds monitored by NMR in the intracrystalline space as the "adsorbed phase". Products were analyzed using a high-resolution gas chromatograph. A sample of SAPO-34 was prepared

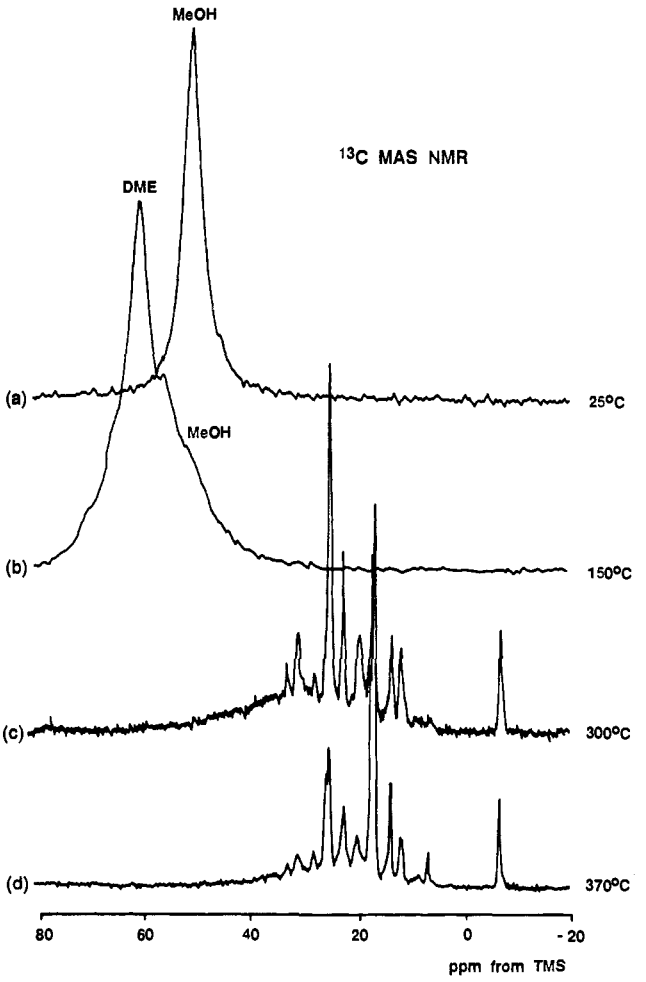

Figure 18. ^{13}C MAS NMR spectra with high-power proton decoupling of the SAPO-34 samples:[135] (a) after adsorption of methanol and no thermal treatment; (b) after heating to 150 °C; (c) after heating to 300 °C for 15 min; (d) after heating to 370 °C for 10 min.

with a chemical formula of $SiAl_6P_5O_{24}$.

Figure 18 shows the ^{13}C MAS NMR spectra recorded after reaction at different temperatures. After adsorption of MeOH and no thermal treatment a single signal at 50 ppm from TMS is observed (Figure 18a). After heating to 150 °C, a rather poorly resolved spectrum is obtained (Figure 18b) consisting of two signals. No further changes are found at 250 °C but after heating to 300 °C for 15 min and 370 °C for 10 min a multitude of narrow resonances are observed in the aliphatic region (−10 to +40 ppm) (Figure 18, parts c and d). No other signals are found. Spectral deconvolution of these resonances, shown in Figure 19, was performed by reference to literature values of ^{13}C NMR chemical shifts.[138]

At 300 °C the most abundant species in the adsorbed phase are isopentane, propane, isobutane, methane, and *n*-butane with less ethane, neopentane, C_6, and C_7 species. At 370 °C the composition of the adsorbed phase is similar except that propane is now more abundant than isopentane. The relative concentrations of adsorbed species were calculated from spectra acquired with high-power proton decoupling but without cross-polarization. Unlike in the case of zeolite H-ZSM-5 (see above) no carbon monoxide intermediate and no aromatics are observed by NMR at any temperature.

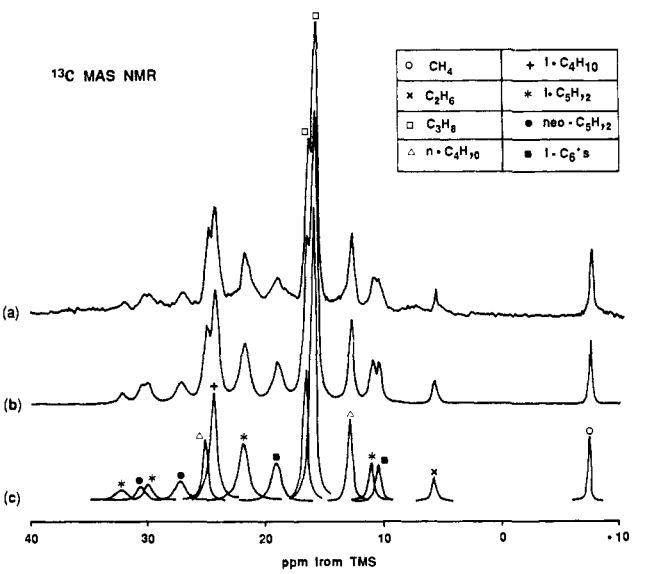

Figure 19. The ^{13}C MAS NMR spectrum[135] of the sample of SAPO-34 with adsorbed methanol treated at 370 °C for 10 min given in a can be simulated (b) using ^{13}C signals corresponding to individual hydrocarbon species (c).

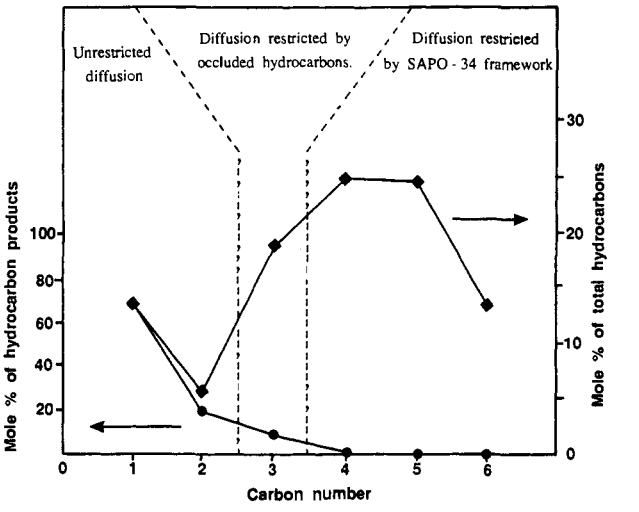

Figure 20. Plot of concentrations of C_1 to C_6 hydrocarbons at 300 °C in the gaseous products determined by gas chromatography (GC) and total hydrocarbons determined by NMR.[135] GC data are for LHSV = 0.3 h^{-1}. NMR and GC data are adjusted so that the concentrations of methane coincide.

The framework structure of SAPO-34 consists of hexagonal prisms (D6R units) linked by four-membered rings in an ABCABC packing sequence (see Figure 17). This results in a three-dimensional channel system and a structure containing large ellipsoidal cages 11 Å long and 6.5 Å wide. The cages are stacked in a hexagonal arrangement forming a three-dimensional network of cages linked by the narrower eight-membered windows. The cage and window dimensions for SAPO-34 are almost identical to those in chabazite and therefore similar molecular sieving properties can be expected. Entrance to the chabazite cages may only be gained through the eight-membered ring windows which are nearly circular with a diameter of approximately 3.8 Å. At room temperature chabazite very rapidly sorbs CH_4 and C_2H_6, slowly sorbs *n*-alkanes but completely excludes branched alkanes.

^{13}C MAS NMR indicates that after heating to 300 °C MeOH and DME are completely converted to aliphatic

hydrocarbons; no olefins are found. This is understood by reference to the gas chromatography results which show that at lower space velocities the products contain a smaller amount of olefins (Figure 20). By extrapolating the data we predict that under static reactor conditions little or no olefins will be formed. A careful inspection of the chromatography results indicates that the relative amounts of C_1, C_2, C_3, C_4, etc. species (olefins + alphatics) are roughly similar irrespective of space velocity. In other words, space velocity does not change oligomerization properties, but it does alter the extent of hydrogenation of products. NMR results, which give a fair representation of the total concentration of species formed in the adsorbed phase, can therefore be compared with their concentration in the gaseous products.

The most striking difference between the composition of the adsorbed phase and the products is the preponderance of branched aliphatics up to C_6 in the former. The effect is so clear as to amount to a textbook example of product shape selectivity. Early work has shown that these branched aliphatics are not sorbed by the chabazite crystals from the gas phase at room temperature. The same effect occurs here in reverse: branched-chain hydrocarbons formed *inside* SAPO-34 are not capable of leaving the intracrystalline space even at temperatures as high as 370 °C.

Of the C_1, C_2, and C_3 species in the adsorbed phase the concentration of C_3 is always the highest. However, it is C_1 which is the most abundant in the gaseous products, followed by C_2 and C_3 species. The C_1/C_2 concentration ratio in the adsorbed phase is roughly equal to that in the gaseous products at 300 °C. This suggests that C_1 and C_2 species have no difficulty in leaving the SAPO-34 crystallite. On the other hand, only 5–10% of the amount of C_3 found in the adsorbed phase is observed in the gas-phase products. Figure 20 illustrates the relative amounts of C_1–C_6 compounds in the products and in the adsorbed phase. The striking differences between the concentrations of C_1 and C_2 on the one hand and C_3 on the other are not easily explained on the basis of diffusion coefficients of aliphatic hydrocarbons in chabazite. At room temperature the diffusion coefficient of propane is ca. 20 times smaller than for ethane and methane. However, at elevated temperatures, such as 150 °C, the difference disappears almost completely. It follows that at 370 °C the expected diffusion coefficients for methane, ethane, and propane should be of the same order of magnitude with a negligible activation barrier. The exclusion of much of the C_3 fraction from the product must therefore be a result of the additional constraints imposed by the presence of branched hydrocarbons which partially block the pore system and significantly alter the diffusional behavior of other species. This further illustrates the need for knowing the contents of the intracrystalline space of a shape-selective catalyst during the course of the reaction. Since the available free space is modified by the occlusion of product molecules, it is not sufficient to take into account the crystallographic pore dimensions in order to predict shape-selective action.

The discovery that, despite the composition of the gaseous products, SAPO-34 in fact converts methanol more selectively to C_3 than to C_2 hydrocarbons suggests ways to modify the catalyst so as to enable the C_3 species to escape, thus making it more selective for propylene than ethylene. This might be done by preparing the catalyst with occluded material or partial exchange with cations large enough to prevent the formation of branched hydrocarbons. This would in turn allow the C_2 and C_3 species to diffuse more readily through the channel system without obstruction from the higher hydrocarbons. The fact that such a prediction can be made on the strength of MAS NMR in tandem with gas chromatography illustrates the remarkable potential of this two-pronged approach in the design of novel molecular sieve catalysts.

Acknowledgments. I am grateful to Shell Research, Amsterdam, for support, and to Dr. M. W. Anderson, Manchester, for Figures 15 and 16.

References

(1) Cronstedt, A. Fr. *Kongl. Svenska Vetenskaps Acad. Handlingar* **1756**, *17*, 120.
(2) Loewenstein, W. *Am. Mineral.* **1954**, *39*, 92.
(3) Weisz, P. B.; Frilette, V. J. *J. Phys. Chem.* **1960**, *64*, 382.
(4) Argauer, R. J.; Landolt, G. R. U.S. Patent, 3,702,886, 1972.
(5) Wilson, S. T.; Lok, B. M.; Messina, C. A.; Cannan, T. R.; Flanigen, E. M. *J. Am. Chem. Soc.* **1982**, *104*, 1146.
(6) Flanigen, E. M.; Lok, B. M.; Patton, R. L.; Wilson, S. T. *Pure Appl. Chem.* **1986**, *58*, 1351.
(7) Meier, W. M.; Olson, D. H. *Atlas of Zeolite Structure Types*; Butterworths: Sevenoaks, 1988.
(8) Breck, D. W. *Zeolite Molecular Sieves: Structure, Chemistry and Use*; John Wiley and Sons: London, 1974.
(9) Barrer, R. M. *Zeolite and Clay Minerals as Sorbents and Molecular Sieves*; Academic Press: London, 1978.
(10) Barrer, R. M. *Hydrothermal Chemistry of Zeolites*; Academic Press: London, 1982.
(11) Zeolite Chemistry and Catalysis. *ACS Monogr.* **1976**, *171*.
(12) Molecular Sieves—II. *ACS Symp. Ser.* **1977**, *No. 40*.
(13) Naccache, D.; Ben Taarit, Y. *Pure Appl. Chem.* **1980**, *52*, 2175.
(14) Jacobs, P. A. *Carboniogenic Activity of Zeolites*; Elsevier, Amsterdam: 1977.
(15) *Catalysis by Zeolites*; Imelik, B., Naccache, C., Ben Taarit, Y., Védrine, J. C., Coudurier, G., Praliaud, H., Eds.; Elsevier: Amsterdam, 1980.
(16) Wasylishen, R. E.; Fyfe, C. A. *Annual Reports on NMR Spectroscopy*; Webb, G. A., Ed.; Academic Press: London, 1982; Vol. 12, pp 1–80.
(17) Klinowski, J. *Progr. NMR Spectrosc.* **1984**, *16*, 237.
(18) Klinowski, J. *Ann. Rev. Mater. Sci.* **1988**, *18*, 189.
(19) Engelhardt, G.; Michel, D. *High-resolution Solid-State NMR of Silicates and Zeolites*; Wiley: Chichester, 1987.
(20) Lippmaa, E.; Mägi, M.; Samoson, A.; Engelhardt, G.; Grimmer, A.-R. *J. Am. Chem. Soc.* **1980**, *102*, 4889.
(21) Samoson, A.; Lippmaa, E. *Phys. Rev.* **1983**, *B28*, 6565.
(22) Samoson, A.; Lippmaa, E. *Chem. Phys. Lett.* **1983**, *100*, 205.
(23) Man, P. P. *J. Magn. Reson.* **1986**, *67*, 78.
(24) Man, P. P. *J. Magn. Reson.* **1988**, *77*, 148.
(25) Man, P. P.; Klinowski, J. *Chem. Phys. Lett.* **1988**, *147*, 581.
(26) Man, P. P.; Klinowski, J.; Trokiner, A.; Zanni, H.; Papon, P. *Chem. Phys. Lett.* **1988**, *151*, 143.
(27) Samoson, A.; Lippmaa, E.; Pines, A. *Mol. Phys.* **1988**, *65*, 1013.
(28) Llor, A.; Virlet, J. *Chem. Phys. Lett.* **1988**, *152*, 248.
(29) (a) Wu, Y.; Chmelka, B. F.; Pines, A.; Davis, M. E.; Grobet, P. J.; Jacobs, P. A. *Nature* **1990**, *346*, 550. (b) Barrie, P. J.; Smith, M. E.; Klinowski, J. *Chem. Phys. Lett.* **1991**, *180*, 6.
(30) Engelhardt, G.; Lohse, U.; Lippmaa, E.; Tarmak, M.; Mägi, M. *Z. Anorg. Allg. Chem.* **1981**, *482*, 49.
(31) Thomas, J. M.; Fyfe, C. A.; Ramdas, S.; Klinowski, J.; Gobbi, G. C. *J. Phys. Chem.* **1982**, *86*, 3061.
(32) Klinowski, J.; Anderson, M. W. *J. Chem. Soc. Faraday Trans. 1* **1986**, *82*, 569.
(33) Jarman, R. H.; Jacobson, A. J.; Melchior, M. T. *J. Phys. Chem.* **1984**, *88*, 5748.
(34) Klinowski, J.; Ramdas, S.; Thomas, J. M.; Fyfe, C. A.; Hartman, J. S. *J. Chem. Soc. Faraday Trans. 2* **1982**, *78*, 1025.
(35) Melchior, M. T.; Vaughan, D. E. W.; Jacobson, A. J. *J. Am. Chem. Soc.* **1982**, *104*, 4859.
(36) Fyfe, C. A.; Gobbi, G. C.; Klinowski, J.; Thomas, J. M.; Ramdas, S. *Nature* **1982**, *296*, 530.
(37) Fyfe, C. A.; O'Brien, J. H.; Strobl, H. *Nature* **1987**, *326*, 281.

(38) Klinowski, J.; Carpenter, T. A.; Gladden, L. F. *Zeolites* **1987**, *7*, 73.
(39) Strobl, H.; Fyfe, C. A.; Kokotailo, G. T.; Pasztor, C. T. *J. Am. Chem. Soc.* **1987**, *109*, 4733.
(40) Hay, D. G.; Jaeger, H.; West, G. W. *J. Phys. Chem.* **1985**, *89*, 107.
(41) West, G. W. *Aust. J. Chem.* **1984**, *37*, 455.
(42) Fyfe, C. A.; Kennedy, G. J.; DeSchutter, C. T.; Kokotailo, G. T. *J. Chem. Soc., Chem. Commun.* **1984**, 541.
(43) Fyfe, C. A.; Gobbi, G. C.; Kennedy, G. J.; Graham, J. D.; Ozubko, R. S.; Murphy, W. J.; Bothner-By, A.; Dadok, J.; Chesnick, A. S. *Zeolites* **1985**, *5*, 179.
(44) Fyfe, C. A.; Gies, H.; Feng, Y. *J. Chem. Soc. Chem. Commun.* **1989**, 1240.
(45) Fyfe, C. A.; Gies, H.; Feng, Y. *J. Am. Chem. Soc.* **1989**, *111*, 7702.
(46) Fyfe, C. A.; Feng, Y.; Kokotailo, G. T. *Nature* **1989**, *341*, 223.
(47) Fyfe, C. A.; Feng, Y.; Gies, H.; Grondey, H.; Kokotailo, G. T. *J. Am. Chem. Soc.* **1990**, *112*, 3264.
(48) Fyfe, C. A.; Grondey, H.; Feng, Y.; Kokotailo, G. T. *J. Am. Chem. Soc.* **1990**, *112*, 8812.
(49) Fyfe, C. A.; Gies, H.; Feng, Y.; Grondey, H. *Zeolites* **1990**, *10*, 278.
(50) Bax, A.; Freeman, R. *J. Magn. Reson.* **1981**, *44*, 542.
(51) Bax, A.; Freeman, R.; Kempsell, S. P. *J. Am. Chem. Soc.* **1980**, *102*, 4849.
(52) Bax, A.; Kempsell, S. P.; Freeman, R. *J. Magn. Reson.* **1980**, *41*, 349.
(53) Buddrus, J.; Bauer, H. *Angew. Chem., Int. Ed. Engl.* **1987**, *26*, 625.
(54) Fyfe, C. A.; Grondey, H.; Feng, Y.; Kokotailo, G. T. *Chem. Phys. Lett.* **1990**, *173*, 211.
(55) Melchior, M. T. *ACS Symp. Ser.* **1983**, *218*, 243.
(56) Hamdan, H.; Klinowski, J. *Chem. Phys. Lett.* **1987**, *139*, 576.
(57) Klinowski, J.; Carpenter, T. A.; Thomas, J. M. *J. Chem. Soc., Chem. Commun.* **1986**, 956.
(58) Haase, J.; Pfeifer, H.; Oehme, W.; Freude, D.; Klinowski, J. *Chem. Phys. Lett.* **1988**, *150*, 189.
(59) McDaniel, C. V.; Maher, P. K. *Molecular Sieves*; Society of Chemical Industry: London, 1968; p 186. Zeolite Chemistry and Catalysis. *ACS Monogr.* **1976**, *171*, 285.
(60) Klinowski, J.; Thomas, J. M.; Fyfe, C. A.; Gobbi, G. C. *Nature* **1982**, *296*, 533.
(61) Maxwell, I. E.; van Erp, W. A.; Hays, G. R.; Couperus, T.; Huis, R.; Clague, A. D. H. *J. Chem. Soc., Chem. Commun.* **1982**, 523.
(62) Engelhardt, G.; Lohse, U.; Samoson, A.; Mägi, M.; Tarmak, M.; Lippmaa, E. *Zeolites* **1982**, *2*, 59.
(63) Engelhardt, G.; Lohse, U.; Patzelová, V.; Mägi, M.; Lippmaa, E. *Zeolites* **1983**, *3*, 233.
(64) Engelhardt, G.; Lohse, U.; Patzelová, V.; Mägi, M.; Lippmaa, E. *Zeolites* **1983**, *3*, 239.
(65) Bosáček, V.; Freude, D.; Fröhlich, T.; Pfeifer, H.; Schmiedel, H. *J. Colloid Interface Sci.* **1982**, *85*, 502.
(66) Freude, D.; Fröhlich, T.; Pfeifer, H.; Scheler, G. *Zeolites* **1983**, *3*, 171.
(67) Freude, D.; Fröhlich, T.; Hunger, M.; Pfeifer, H.; Scheler, G. *Chem. Phys. Lett.* **1983**, *98*, 263.
(68) Freude, D.; Hunger, M.; Pfeifer, H. *Chem. Phys. Lett.* **1982**, *91*, 307.
(69) Klinowski, J.; Fyfe, C. A.; Gobbi, G. C. *J. Chem. Soc., Faraday Trans. 1* **1985**, *81*, 3003.
(70) Lohse, U.; Stach, H.; Thamm, H.; Schirmer, W.; Isirikian, A. A.; Regent, N. I.; Dubinin, M. M. *Z. Anorg. Allg. Chem.* **1980**, *460*, 179.
(71) Lohse, U.; Mildebrath, M. *Z. Anorg. Allg. Chem.* **1981**, *476*, 126.
(72) Dwyer, J.; Fitch, F. R.; Machado, F.; Qin, G.; Smyth, S. M.; Vickerman, J. C. *J. Chem. Soc., Chem. Commun.* **1981**, 423.
(73) Dwyer, J.; Fitch, F. R.; Qin, G.; Vickerman, J. C. *J. Phys. Chem.* **1982**, *86*, 4574.
(74) Ward, M. B.; Lunsford, J. H. *J. Catal.* **1984**, *87*, 524.
(75) Kellberg, L.; Linsten, M.; Jakobsen, H. J. *Chem. Phys. Lett.* **1991**, *182*, 120.
(76) Rocha, J.; Klinowski, J. *J. Chem. Soc., Chem. Commun.* **1991**, 1121.
(77) Rocha, J.; Klinowski, J. *J. Am. Chem. Soc.*, submitted for publication.
(78) Samoson, A.; Lippmaa, E.; Engelhardt, G.; Lohse, U.; Jerschkewitz, H.-G. *Chem. Phys. Lett.* **1987**, *134*, 589.
(79) Hamdan, H.; Klinowski, J. *ACS Symp. Ser.* **1989**, *No. 398*, 448; 465.
(80) Tijink, G. A. H.; Janssen, R.; Veeman, W. S. *J. Am. Chem. Soc.* **1987**, *109*, 7301.
(81) Hamdan, H.; Klinowski, J. *J. Chem. Soc., Chem. Commun.* **1989**, 240.
(82) Gilson, J.; Edwards, G. C.; Peters, A. W.; Rajagopalan, K.; Wormsbecher, R. F.; Roberie, T. G.; Shatlock, M. P. *J. Chem. Soc., Chem. Commun.* **1987**, 91.
(83) Alemany, L. B.; Kirker, G. W. *J. Am. Chem. Soc.* **1986**, *108*, 6158.
(84) Hamdan, H.; Sulikowski, B.; Klinowski, J. *J. Phys. Chem.* **1989**, *93*, 350.
(85) Barrie, P. J.; Gladden, L. F.; Klinowski, J. *J. Chem. Soc., Chem. Commun.* **1991**, 592.
(86) Freude, D.; Hunger, M.; Pfeifer, H.; Schwieger, W. *Chem. Phys. Lett.* **1986**, *128*, 62.
(87) Freude, D.; Hunger, M.; Pfeifer, H. *Chem. Phys. Lett.* **1982**, *91*, 307.
(88) Freude, D.; Klinowski, J.; Hamdan, H. *Chem. Phys. Lett.* **1988**, *149*, 355.
(89) Freude, D.; Klinowski, J. *J. Chem. Soc., Chem. Commun.* **1988**, 1411.
(90) van Vleck, J. H. *Phys. Rev.* **1948**, *74*, 1168.
(91) Freude, D. *Adv. Coll. Interface Sci.* **1985**, *23*, 21.
(92) Böhm, J.; Fenzke, D.; Pfeifer, H. *J. Magn. Reson.* **1983**, *55*, 197.
(93) Vega, A. J.; Luz, Z. *J. Phys. Chem.* **1987**, *91*, 365.
(94) Batamack, P.; Dorémieux-Morin, C.; Fraissard, J.; Freude, D. *J. Phys. Chem.* **1991**, *95*, 3790.
(95) Scholle, K. F. M. G. J.; Veeman, W. S.; Post, J. G.; van Hooff, J. H. C. *Zeolites* **1983**, *3*, 214.
(96) Scholle, K. F. M. G. J.; Kentgens, A. P. M.; Veeman, W. S.; Frenken, P.; van der Velden, G. P. M. *J. Phys. Chem.* **1984**, *88*, 5.
(97) Michel, D.; Germanus, A.; Scheler, D.; Thomas, B. *Z. Phys. Chem. (Leipzig)* **1981**, *262*, 113.
(98) Michel, D.; Germanus, A.; Pfeifer, H. *J. Chem. Soc., Faraday Trans. 1* **1982**, *78*, 237.
(99) Jünger, I.; Meiler, W.; Pfeifer, H. *Zeolites* **1982**, *2*, 310.
(100) Rothwell, W. P.; Shen, W.; Lunsford, J. H. *J. Am. Chem. Soc.* **1984**, *106*, 2452.
(101) Lunsford, J. H.; Rothwell, W. P.; Shen, W. *J. Am. Chem. Soc.* **1985**, *107*, 1540.
(102) Meisel, S. L.; McCullogh, J. P.; Lechthaler, C. H.; Weisz, P. B. *CHEMTECH* **1976**, *6*, 86.
(103) Kaeding, W. W.; Butter, S. U.S. Patent No. 3,911,041, 1975.
(104) Chang, C. D. *Catal. Rev. Sci. Eng.* **1983**, *25*, 1.
(105) Winde, G.; Volkov, A. V.; Kiselev, A. V.; Lygin, V. I. *Russian J. Phys. Chem.* **1975**, *49*, 1716.
(106) Luz, Z.; Vega, A. J. *J. Phys. Chem.* **1987**, *91*, 374.
(107) Mirth, G.; Lercher, J. A.; Anderson, M. W.; Klinowski, J. *J. Chem. Soc., Faraday Trans.* **1990**, *86*, 3039.
(108) Anderson, M. W.; Barrie, P. J.; Klinowski, J. *J. Phys. Chem.* **1991**, *95*, 235.
(109) Carpenter, T. A.; Klinowski, J.; Tennakoon, D. T. B.; Smith, C. J.; Edwards, D. C. *J. Magn. Res.* **1986**, *68*, 561.
(110) Anderson, M. W.; Klinowski, J. *J. Chem. Soc., Chem. Commun.* **1990**, 918.
(111) Anderson, M. W.; Klinowski, J. *Nature* **1989**, *339*, 200.
(112) Anderson, M. W.; Klinowski, J. *J. Am. Chem. Soc.* **1990**, *112*, 10.
(113) Richardson, B. R.; Lazo, N. D.; Schettler, P. D.; White, J. L.; Haw, J. F. *J. Am. Chem. Soc.* **1990**, *112*, 2885.
(114) Lazo, N. D.; White, J. L.; Munson, E. J.; Lambregts, M.; Haw, J. F. *J. Am. Chem. Soc.* **1990**, *112*, 4050.
(115) White, J. L.; Lazo, N. D.; Richardson, B. R.; Haw, J. F. *J. Catal.* **1990**, *125*, 260.
(116) Munson, E. J.; Haw, J. F. *Anal. Chem.* **1990**, *62*, 2532.
(117) Munson, E. J.; Lazo, N. D.; Moellenhoff, M. E.; Haw, J. F. *J. Am. Chem. Soc.* **1991**, *113*, 2783.
(118) Anderson, M. W.; Occelli, M. L.; Klinowski, J. *J. Phys. Chem.* (in press).
(119) Haw, J. F.; Richardson, B. R.; Oshiro, I. S.; Lazo, N. D.; Speed, J. A. *J. Am. Chem. Soc.* **1989**, *111*, 2052.
(120) Csicsery, S. M. Zeolite Chemistry and Catalysis. *ACS Monogr.* **1976**, *171*, 680.
(121) Chen, N. Y.; Kaeding, W. W.; Dwyer, F. G. *J. Am. Chem. Soc.* **1979**, *101*, 6783.
(122) Kaeding, W. W. U.S. Patent No. 4,029,716, 1977.
(123) Haag, W. O.; Olson, D. H. U.S. Patent No. 4,097,543, 1978.
(124) Derouane, E. G.; Nagy, J. B.; Dejaifve, P.; van Hooff, J. H. C.; Spekman, B. P.; Védrine, J. C.; Naccache, C. *J. Catal.* **1978**, *53*, 40.
(125) Derouane, E. G.; Dejaifve, P.; Nagy, J. B.; van Hooff, J. H. C.; Spekman, B. P.; Naccache, C.; Védrine, J. C. *CR Acad. Sci. Paris Ser. C* **1977**, *284*, 945.
(126) Nagy, J. B.; Gilson, J. P.; Derouane, E. G. *J. Mol. Catal.* **1979**, *5*, 393.
(127) Derouane, E. G.; Dejaifve, P.; Nagy, J. B. *J. Mol. Catal.* **1977**, *3*, 453.
(128) Derouane, E. G.; Nagy, J. B. *ACS Symp. Ser.* **1984**, *No. 248*, 101.
(129) Derouane, E. G.; Gilson, J. P.; Nagy, J. B. *Zeolites* **1982**, *2*, 42.
(130) Bronnimann, C. E.; Maciel, G. E. *J. Am. Chem. Soc.* **1986**, *108*, 7154.
(131) Stothers, J. B. *Carbon-13 NMR Spectroscopy*; Academic Press: New York, 1972.

(132) Anderson, M. W.; Klinowski, J. *Chem. Phys. Lett.* **1990**, *172*, 275.
(133) Kolodziejski, W.; Klinowski, J. *Chem. Phys. Lett.*, in press.
(134) Aronson, M. T.; Gorte, R. J.; Farneth, W. E.; White, D. *J. Am. Chem. Soc.* **1989**, *111*, 840.
(135) Anderson, M. W.; Sulikowski, B.; Barrie, P. J.; Klinowski, J. *J. Phys. Chem.* **1990**, *94*, 2730.
(136) Lok, B. M.; Messina, C. A.; Patton, R. L.; Gajek, R. T.; Cannan, T. R.; Flanigen, E. M. *J. Am. Chem. Soc.* **1984**, *106*, 6092.
(137) Ito, M.; Shimoyama, Y.; Saito, Y.; Tsurita, Y.; Otake, M. *Acta Crystallogr.* **1985**, *C41*, 1698.
(138) Kalinowski, H. O.; Berger, S.; Braun, S. *^{13}C-NMR-Spektroskopie*; Georg Thieme: Stuttgart, 1984.